# REPORT DOCUMENTATION PAGE



AFRL-SR-AR-TR-04-

0295

| 1. REPORT DATE (DD-MM-YYYY) | 2. REPORT TYPE | 3. DATES COVERED (From - To) |
|---|---|---|
| 27-05-2004 | Final Performance Report | Sept. 2001 to Dec. 2003 |

**4. TITLE AND SUBTITLE**
Complex-Shaped Microcomponents by the Reactive Conversion of Biological Templates

**5a. CONTRACT NUMBER**

**5b. GRANT NUMBER**
F49620-01-1-0507

**5c. PROGRAM ELEMENT NUMBER**

**6. AUTHOR(S)**
Sandhage, Kenneth, H.

**5d. PROJECT NUMBER**

**5e. TASK NUMBER**

**5f. WORK UNIT NUMBER**

**7. PERFORMING ORGANIZATION NAME(S) AND ADDRESS(ES)**
The Ohio State University
1960 Kenny Road
Columbus, OH 43210

**8. PERFORMING ORGANIZATION REPORT NUMBER**

**9. SPONSORING/MONITORING AGENCY NAME(S) AND ADDRESS(ES)**
Air Force Office of Scientific Research
801 North Randolph Street
Room 732
Arlington, VA 22203-1977

NL

**10. SPONSOR/MONITOR'S ACRONYM(S)**
AFOSR

**11. SPONSOR/MONITOR'S REPORT NUMBER(S)**

**12. DISTRIBUTION/AVAILABILITY STATEMENT**

Approve for Public Release: Distribution Unlimited





**13. SUPPLEMENTARY NOTES**

**14.** This project has been aimed at: 1) identifying gas/solid reaction conditions for converting biologically-derived micro/nanotemplates into other oxides without a loss of the starting 3-D shape and fine features, and 2) evaluating the nanochemical/nanostructural evolution during such reactive conversion. The most significant accomplishments have been:

1) Development of an oxidation-reduction reaction process for converting biosilica-based micro/nanoassemblies into MgO nanoparticle structures with a preservation of the starting 3-D shape and fine features at temperatures as low as 700°C
2) Development of a two-step oxidation-reduction reaction process for converting biosilica-based micro/nanoassemblies into CaO nanoparticle structures with a preservation of the starting 3-D shape and fine features at temperatures as low as 1000°C
3) Development of a two-step metathetic reaction process for converting biosilica-based micro/nanoassemblies into $TiO_2$ nanoparticle structures with a preservation of the starting 3-D shape and fine features at temperatures as low as 350°C
4) Identification of novel reaction paths accessed during conversion of biosilica structures into magnesia (via formation of forsterite as an intermediate product) and titania (via formation of the intermediate compound, titanium oxyfluoride)
5) Identification of peptides that promote room-temperature formation of germania nanoparticle networks

**15. SUBJECT TERMS**

| 16. SECURITY CLASSIFICATION OF: | | | 17. LIMITATION OF ABSTRACT | 18. NUMBER OF PAGES | 19a. NAME OF RESPONSIBLE PERSON |
|---|---|---|---|---|---|
| a. REPORT | b. ABSTRACT | c. THIS PAGE | | | 19b. TELEPHONE NUMBER (Include area code) |

**Final Performance Report**

| | |
|---|---|
| **Project Title:** | Complex-Shaped Microcomponents by the Reactive Conversion of Biological Templates |
| **Award Number:** | F49620-01-1-0507 |
| **Start Date:** | Sept. 15, 2001 |
| **End Date:** | Dec. 15, 2003 (2 year, 3 month duration) |
| **Program Manager:** | Dr. Hugh C. De Long<br>Program Manager<br>Biomimetics, Biomaterials, and Biointerfacial Sciences<br>Air Force Office of Scientific Research<br>801 N. Randolph St., Room 732<br>Arlington, VA 22203-1977<br>E-mail: hugh.delong@afosr.af.mil<br>Phone: :(703) 696-7722<br>Fax: (703) 696-8449 |
| **Principal Investigator:** | Prof. Ken H. Sandhage<br>School of Materials Science & Engineering<br>Georgia Institute of Technology<br>771 Ferst Drive<br>Atlanta, GA 30332-0245<br>E-mail: ken.sandhage@mse.gatech.edu<br>Phone: (404) 894-6882<br>Fax: (404) 894-9140 |
| **Co-Investigators:** | Dr. Rajesh Naik, Dr. Morley Stone<br>Biotechnology Group, MLPJ Hardened Materials Branch<br>Air Force Research Laboratory, Wright-Patterson AFB<br>3005 P Street<br>WPAFB, OH 45433-7702<br>E-mail: morley.stone@afrl.af.mil<br>Phone: (937) 255-3808 ext. 3180<br>Fax: (937) 255-1128 |

## Executive Summary

Nature provides numerous examples of organisms that directly generate intricate 3-D mineralized (bioclastic) structures with micro-to-nanoscale features. Perhaps the most spectacular example is the single-celled aquatic algae known as the diatom. Diatoms assemble amorphous silica nanoparticles into intricate microshells (frustules) with a dazzling variety of shapes. Indeed, each of the estimated $10^5$ extant diatom species generates a frustule with a unique 3-D shape and with specific patterns of fine features (e.g., regularly-spaced $10^2$ nm pores, channels, ridges). Because the shapes and fine features on the frustules are reproduced with fidelity from generation to generation, sustained reproduction can yield enormous numbers of similarly-shaped assemblies (e.g., 40 sequential reproduction cycles would yield $2^{40}$ or >1 trillion copies). Such massively-parallel, precise, and direct self-assembly of complex 3-D micro/nano-structures has no synthetic analog. However, the silica-based chemistry of diatom frustules greatly limits the range of potential device applications for such micro/nanostructures. This research project has been focused on the use of the **BaSIC** (**B**ioclastic **a**nd **S**hape-preserving **I**norganic **C**onversion) process to overcome this natural limitation. With this process, gas/silica displacement reactions are used to convert biosilica preforms into new oxide compositions.

This bio-inspired research project has been aimed at: 1) identifying reaction conditions that enable biologically-derived micro/nanotemplates to be fully converted into other oxides without a loss of the starting 3-D shape and fine features, and 2) developing a better understanding of the manner in which the nanochemistry and nanostructure of biologically-derived 3-D micro/nano-templates evolve during the course of reactive conversion.

The most significant accomplishments of this research project have been:

1) Development of a single heat treatment oxidation-reduction reaction process that enables bioclastic and biosculpted $SiO_2$-based micro/nanoassemblies to be converted into MgO nanoparticle structures with a preservation of the starting 3-D shape and fine features at temperatures as low as 700°C
2) Development of a two-step oxidation-reduction reaction process that enables bioclastic $SiO_2$-based micro/nanoassemblies to be converted into CaO nanoparticle structures with a preservation of the starting 3-D shape and fine features at temperatures as low as 1000°C
3) Development of a two-step metathetic reaction process for converting bioclastic $SiO_2$-based micro/nanoassemblies into $TiO_2$ (anatase) nanoparticle structures with a preservation of the starting 3-D shape and fine features at temperatures as low as 350°C
4) Identification of novel reaction paths accessed during the conversion of biosilica structures into magnesia (via the formation of forsterite as an intermediate product) and titania (via the formation of the intermediate compound, titanium oxyfluoride)
5) Isolation and identification of peptides that promote the room-temperature formation of germania nanoparticle networks

The graduate students who have been involved in this research at Ohio State University (OSU) and the Georgia Institute of Technology (GIT) are:

Mr. Shawn Allan (GIT)
Mr. Matthew Dickerson (OSU and GIT)
Mr. Kushagra Pathak (OSU)
Mr. Samuel Shian (OSU and GIT)
Mr. Raymond Unocic (OSU)
Mr. Frank Zalar (OSU)

Mr. Frank Zalar obtained his M.S. degree ("Shape-preserving Conversion of $SiO_2$-based Bioclastic Structures into MgO and CaO via the BaSIC Process") during this research project.

Publications stemming from this research include:

1. M. B. Dickerson, R. R., Naik, P. M Sarosi, G. Agarwal, M. O. Stone, K. H. Sandhage, "Ceramic Nanoparticle Assemblies with Tailored Shapes and Tailored Chemistries via Biosculpting and Shape-preserving Inorganic Conversion," J. Nanosci. Nanotech., accepted, in press.
2. M. B. Dickerson, R. R. Naik, M. O. Stone, Y. Cai, and K. H. Sandhage, "Identification of Peptides that Promote the Rapid Precipitation of Germania Nanoparticle Networks via Use of a Peptide Display Library," Chem. Comm., accepted, in press.
3. R. R. Unocic, Frank M. Zalar, Peter M. Sarosi, Ye Cai, and K. H. Sandhage, "Anatase Assemblies from Algae: Coupling Biological Self-assembly of 3-D Nanoparticle Structures with Synthetic Reaction Chemistry," Chem. Comm., [7] 795-796 (2004).
   ***(Selected as a "hot paper" for this edition of Chemical Communications)***
4. F. M. Zalar, M. B. Dickerson, and K. H. Sandhage, "Self-Assembled, 3-D Nanoparticle Structures with Tailored Chemistries via the BaSIC Process," pp. 415-422 in Processing and Fabrication of Advanced Materials XI, Vol. 2, Eds. T. S. Srivatsan, R. A. Varin, ASM International, Materials Park, OH (2003).
5. J. Nash, M. B. Dickerson, K. Pathak, K. H. Sandhage, R. L. Snyder, U. Balachandran, B. Ma, R. Blaugher, R. Bhattacharya, "Novel, Closed Heating Chambers for Rapid, In-Situ, HTXRD Analyses of Gas/Solid and Liquid/Solid Reactions," pp. 44-52 in Processing and Fabrication of Advanced Materials XI, Vol. 2, Eds. T. S. Srivatsan, R. A. Varin, ASM International, Materials Park, OH (2003).
6. K. H. Sandhage, M. B. Dickerson, P. M. Huseman, F. M. Zalar, M. R. Rondon, E. C. Sandhage, "A Novel Hybrid Route to Chemically-Tailored, Three-Dimensional Oxide Nanostructures: The BaSIC (Bioclastic and Shape-Preserving Inorganic Conversion) Process," Ceram. Eng. Sci. Proc., 23 [4] 653-664 (2002).
7. K. H. Sandhage, M. B. Dickerson, P. M. Huseman, M. A. Caranna, J. D. Clifton, T. A. Bull, T. J. Heibel, W. R. Overton, M. E. A. Schoenwaelder, "Novel, Bioclastic Route to Self-Assembled, 3D, Chemically Tailored Meso/Nanostructures: Shape-Preserving Reactive Conversion of Biosilica (Diatom) Microshells," Adv. Mater., **14** [6] 429-433 (2002).
8. K. H. Sandhage, M. B. Dickerson, P. M. Huseman, F. M. Zalar, M. R. Rondon, E. C. Sandhage, "A Novel Hybrid Route to Chemically-Tailored, Three-Dimensional Oxide Nanostructures: The BaSIC (Bioclastic and Shape-Preserving Inorganic Conversion) Process," Progress in Nanotechnology., pp. 255-266, The American Ceramic Society, Westerville, OH (2002).

These publications have also been specifically cited in third author articles by ScienceNow ("Turning Diatoms into Nanodevices," March 18, 2002), Wissenschaft-online ("After the Model of Nature," March 20, 2002), Bild am Sonntag ("Algen: Die Powerpflanzen der Zukunft," Jan. 26, 2003), Nanotechweb.org ("Diatomists Shell Out on Nanotechnology," Features Section, February 21, 2003), Nano/Bio Convergence News ("Diatoms: The Next Nanotechnologists,", Section on Biomimetics; Vol. 1, No. 7, March 2003), New Scientist ("Natural Glass," pp. 26-29, Jan. 17, 2004), Nature Materials ("Recasting Natural Nanostructures," in Nanozone section of Materials Update on Nature Materials website, May 13, 2004), Chemical Science ("Technological Advance from Nature's Design,", Vol. 1, Issue 5, pg. C36, May 2004), and Materials Connections ("Silica in Naturally Occurring Nanostructures Replaced with Titania," MRS website, May 26, 2004).

## Objectives

The objectives of this bio-inspired research project have been:

1) to identify reaction conditions that enable biologically-derived micro/nanotemplates to be fully converted into other oxides without a loss of the starting 3-D shape and fine features, and

2) to develop a better understanding of the manner in which the nanostructure and nanochemistry of biologically-derived 3-D micro/nanotemplates evolve during the course of reactive conversion.

## Technical Summary

This collaborative OSU/WPAFB research project (Sandhage (PI), Naik (co-PI), Stone (co-PI)) has focused on the chemical conversion of biosilica structures by the following net gas/solid displacement reactions:

Oxidation-Reduction Reactions:

$$2Mg(g) + SiO_2(s) \Rightarrow 2MgO(s) + \{Si\} \quad (1)$$

$$2Ca(g) + SiO_2(s) \Rightarrow 2CaO(s) + \{Si\} \quad (2)$$

Metathetic Reaction:

$$TiF_4(g) + SiO_2(s) \Rightarrow TiO_2(s) + SiF_4(g) \quad (3)$$

where {Si} refers to Si in a Mg-Si or Ca-Si liquid. Two types of silica nanoparticle structures have been converted in this work: i) bioclastic structures (i.e., diatom microshells, called frustules), and ii) biosculpted structures produced with the use of silaffin-based precipitation agents (silaffins are peptides obtained from diatoms). Research has also been conducted to isolate and identify peptides that promote the formation of germania, $GeO_2$. The thermodynamic driving force for the reactive conversion of $GeO_2$ into a given new oxide is much larger than for the reactive conversion of $SiO_2$ into the same new oxide. Hence, identification of germania-forming peptides enables the biosculpting of germania preforms and then reactive conversion into a wider variety of oxides than is thermodynamically possible with silica preforms.

In the following technical summary, the bioclastic and biosculpted silica preforms will first be described. In the next three sections, the reactive conversion of biosilica preforms into magnesia, calcia, and titania will be discussed. In the final section, research on the isolation and identification of germania-forming peptides is summarized.

### I. Bioclastic and Biosculpted Silica Preforms

The bioclastic structures used in the present work are the frustules (microshells) of diatoms. Secondary electron images of frustules of the diatom *Aulacoseira* are shown in Figs. 1a-c. The *Aulacoseira* frustule is a hollow cylinder with fine ($10^2$ nm) pores running in rows along the cylinder length. As for all diatoms, the *Aulacoseira* frustule contains two halves. One end of

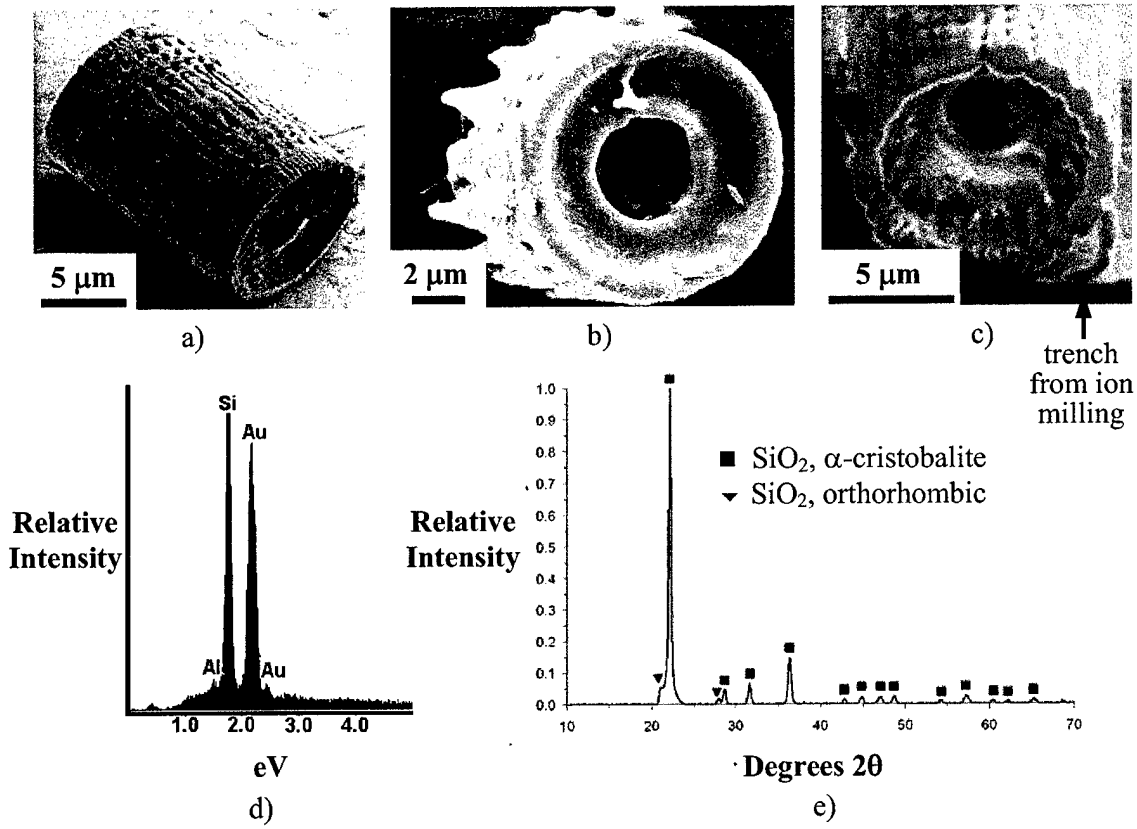


Figure 1. a)-c) Secondary electron (SE) images obtained from *Aulacoseira* frustules. A complete frustule pair is shown in a), whereas a half of this frustule pair is shown in b). The thickness of the frustule wall, and features present on inside surfaces of the frustule, can be seen in the partially-milled frustule in c). EDX and XRD analyses of the starting *Aulacoseira* frustules are shown in d) and e), respectively (note: the Au peak in Fig. 1d was due to a gold coating applied to the frustule to avoid charging in the electron microscope; the small Al peak was due to the substrate on which the specimen was resting).

each half is open, whereas the other end is closed and exhibits fingerlike protuberances (the open end of a half frustule can be seen in Figure 1b). The fingerlike protuberances from the closed ends of two half frustules interlock to form a complete frustule (see Figure 1a). Partial removal of the end of an *Aulacoseira* frustule by ion milling (see Figure 1c) revealed that the frustule wall was about 1.3 μm thick at positions located away from pore channels running through the frustule wall. The only cation detected within the starting frustules by energy-dispersive x-ray (EDX) analysis was silicon (Figure 1d). X-ray diffraction (XRD) analyses (Figure 1e) revealed that the predominant crystalline phase in the starting frustules was α-cristobalite (note: these frustules were obtained from a commercial vendor as diatomaceous earth, which had undergone a flame polishing treatment that lead to cristobalite formation).

Biosculpted silica structures, in the shape of interwoven microfilaments, were also used as preforms for reactive conversion experiments (via collaboration with R. Naik and M. Stone at WPAFB). The R5 repeat segment [SSKKSGSYSGSKGSKRRIL] of the silaffin-1 protein from the diatom *Cylindrotheca fusiformis*[1] was used as a silica-forming agent. A synthetic version of

the R5 peptide was dissolved in a sodium phosphate buffer (pH 7.5) to a final concentration of 10 mg/ml in a microcentrifuge tube. Hydrolyzed tetramethylorthosilicate (TMOS) was prepared by dissolving TMOS in 1 mM HCl to a final concentration of 1 M. The hydrolyzed TMOS was then added to the buffered R5 peptide solution such that the final concentration of TMOS in the reaction was 0.1 M. The reaction mixture was then passed back and forth for *ca.* 5 min at room temperature within a 29 cm length of 1.6 mm internal diameter Tygon tubing, so as to generate a linear shear flow condition.[2] The resulting precipitate was then centrifuged at 14,000 G for 5 min. The precipitate was washed several times with double-distilled deionized water. Silica precipitation under this linear shear flow condition yielded the microfilamentary structure shown in Figure 2a. The silica microfilaments possessed diameters of 0.2 to 1 μm (note: energy-dispersive x-ray analyses confirmed that the microfilaments were comprised of silica). A brightfield transmission electron microscope (TEM) image of a cross-section of the microfilaments is shown in Figure 2b. The latter image revealed that each silica microfilament was bonded to adjacent microfilaments. The higher magnification TEM image in Figure 2c

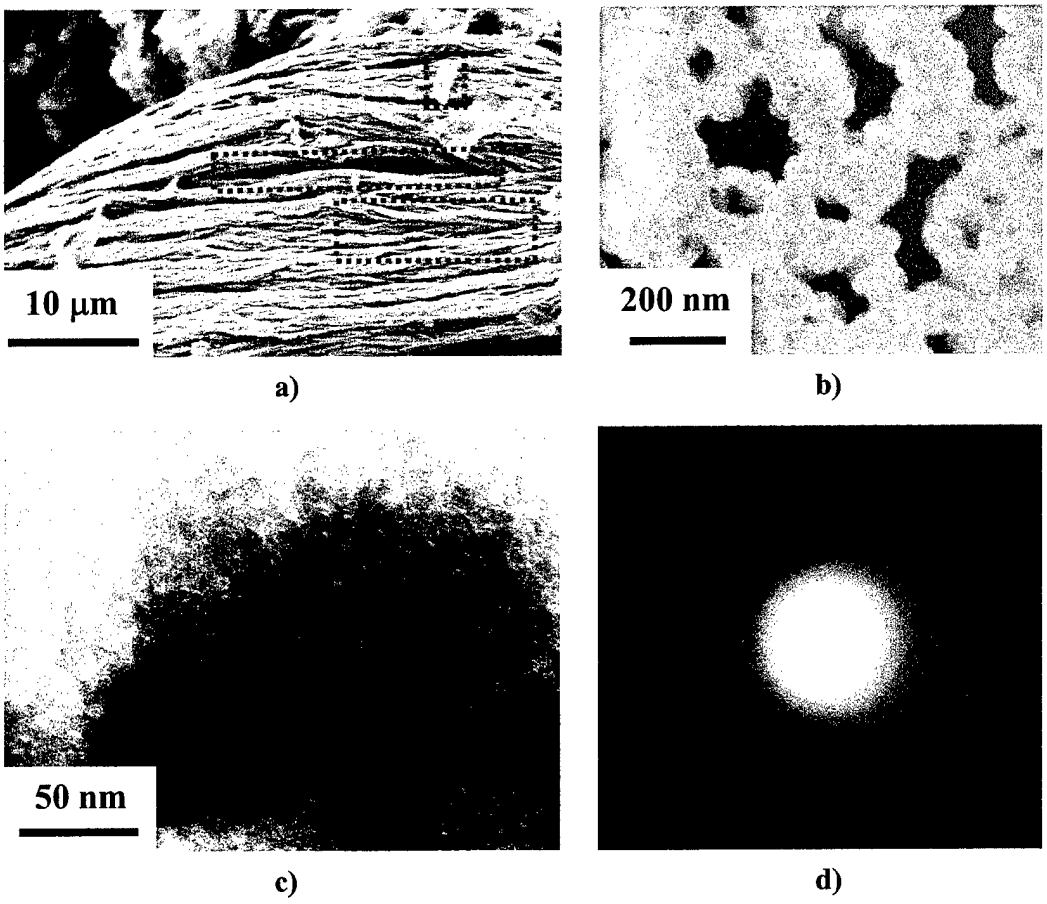


Figure 2. a) Secondary electron image of a biosculpted silica nanoparticle assembly in the form of interwoven microfilaments generated by precipitation from a TMOS solution using a silaffin-derived R5 peptide precipitation agent under a laminar shear flow condition. b), c) Brightfield TEM images and d) electron diffraction pattern obtained from a fractured cross-section of such biosculpted microfilamentary silica.

revealed the presence of nanoparticles (<10 nm in diameter) within each filament. An electron diffraction (ED) pattern of the microfilaments is shown in Figure 2d. The absence of diffraction spots and the presence of diffuse rings in this ED pattern indicated that the microfilaments were comprised of assemblies of amorphous silica nanoparticles.

## II. Reactive Conversion of Bioclastic and Biosculpted Silica into Magnesium Oxide

The *Aulacoseira* diatom frustules and the biosculpted silica microfilaments were sealed (by welding) along with solid magnesium into steel ampoules. (Note: the magnesium was physically separated from the biosilica specimens within the tube.) The sealed tubes were then heated to 650-900°C and held for 0.5-8 hours in a flowing argon atmosphere (to minimize oxidation of the steel tube). Steel was used as a substrate and as an enclosure owing to negligible reaction with magnesium at $\leq$900°C.[3] Upon heating to 650-900°C, magnesium melted, vaporized, and then reacted as a gas with the biosilica specimens inside the ampoule. After cooling to room temperature, the steel ampoule was cut open and the reacted specimens were removed. Secondary electron images of biosculpted specimens before and after reaction were obtained with a Model 1530 LEO field emission gun (FEG) scanning electron microscope. A focused ion beam instrument (Model Strata DB-235 System, FEI Company, Hillsboro, OR) was used to cut electron transparent cross sections from reacted specimens. Brightfield TEM images were obtained with a Model CM-200T FEG transmission electron microscope (Philips Electron Instruments) or Hitachi HF-2000 200kV FEG transmission electron microscope. The scanning electron microscope and transmission electron microscope were both equipped with an energy-dispersive x-ray detector (Edax International, Mahwah, NJ) for local chemical analyses.

Initial experiments were conducted at 900°C. At this temperature, the Mg(g) underwent the following net displacement reaction with $SiO_2$(s) in the frustules:

$$2Mg(g) + SiO_2(s) => 2MgO(s) + \{Si\} \qquad (1)$$

where {Si} refers to Si present in a Mg-Si liquid. The equilibrium vapor pressure of magnesium gas over pure, liquid magnesium at 900°C is 120 torr.[4] At this temperature and magnesium partial pressure, the Gibbs free energy change for reaction (1), with a crystalline silica reactant and with a pure silicon product, is -265.5 kJ/mole.[4] Because the silica in this work was amorphous, and because the silicon product was dissolved in a Mg-Si liquid, this reaction was even more strongly favored. The Mg-Si liquid product of reaction (1), indicated by {Si}, was generated by the continued reaction of magnesium gas with the silicon that formed upon the reduction of silica (note: the solubility of Si in molten Mg at 900°C is 10.5 at%[5]).

Images of the same *Aulacoseira* frustules before and after reaction for 4 hours at 900°C are shown in Figures 3a and 3b, respectively. Comparison of these images reveals that the general shape and fine features of the diatom frustules were retained upon reaction with Mg(g). Ten specific surface features are clearly observed, along with the fine pores, before and after reaction. The solidified Mg-Si product of reaction (1) can be seen below the reacted frustule in Figure 3b (note: the reacted frustule did not adhere well to the solidified Mg-Si, which was consistent with poor wetting of the frustule by the Mg-Si liquid at 900°C). Image analyses indicated that there was no significant difference in the pore size distributions of the *Aulacoseira* frustules before and after reaction with Mg(g); that is, the average pore size remained close to 300 nm before and after reaction. A higher magnification secondary electron image of a reacted frustule is shown in

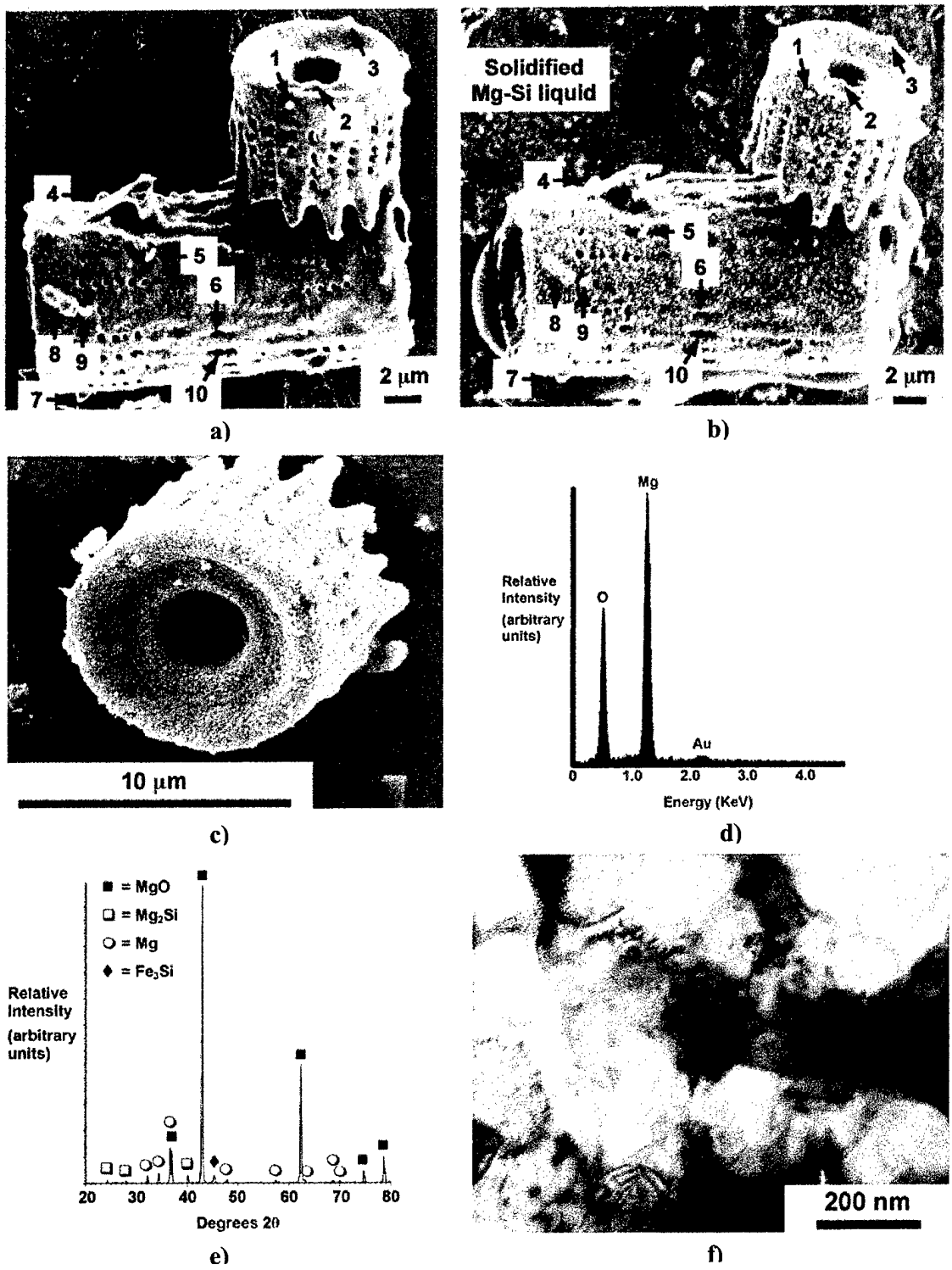


Figure 3. Secondary electron images obtained from *Aulacoseira* frustules: a) before, and b), c) after reaction with Mg(g) for 4 hours at 900°C. d) SEM/EDX pattern from the reacted frustule. e) An XRD pattern and f) a bright field TEM image of a cross-section of such a reacted *Aulacoseira* frustule.

Figure 3c. The surface of the reacted frustule appeared more granular than for the starting frustules shown in Figure 3a, which was consistent with the formation of polycrystalline MgO. An energy-dispersive x-ray spectrum obtained from the reacted frustule is shown in Figure 3d. Strong peaks for Mg and O were observed, which was consistent with complete conversion of $SiO_2$ into MgO within 4 hours at 900°C (note: the weak gold peak in Figure 3d was a result of a conductive coating applied to the reacted frustule). An x-ray diffraction (XRD) pattern obtained from such reacted diatoms (Figure 3e) revealed strong diffraction peaks for MgO, $Mg_2Si$, and Mg, along with a weak peak for $Fe_3Si$. This data was consistent with complete conversion of the silica frustule into MgO. The $Mg_2Si$ and Mg phases were the expected products upon solidification of the Mg-rich, Mg-Si liquid (some of this solidified product was captured with the MgO as the reacted frustules were scraped from the substrate for characterization). The presence of $Fe_3Si$ was a result of the reaction of Si in the Mg-Si liquid with the iron in the substrate (i.e., the iron substrate acted as a reactive surface on which the Mg-Si liquid could wet and spread away from the converted diatom frustules). A TEM bright field image of a cross-section of a fully-reacted frustule (i.e., after exposure to Mg(g) for 4 hours at 900°C) is shown in Figure 3f. TEM/EDX analyses at various locations throughout the specimen cross-section yielded peaks for Mg and O, but not Si. This was consistent with complete removal (via de-wetting) of the Mg-Si liquid product of reaction (1) from the MgO-converted frustule. Hence, x-ray diffraction and electron microscopy (SEM, TEM) confirmed that the Aulacoseira diatom frustules could be fully converted into nanocrystalline MgO within 4 hours of reaction with Mg(g) at 900°C.

Secondary electron images of the same biosculpted microfilamentary silica specimen before and after reaction for 4 hours at 900° are shown in Figures 2a and 4a, respectively. Comparison of these images reveals that the reacted specimen retained the overall shape and interwoven microfilamentary structure of the starting silica specimen. Indeed, the geometries of specific microfilaments and other fine (submicron) features were precisely preserved upon reaction (compare the features within the red boxes in Figures 2a and 4a). A brightfield TEM image of a cross-section of a reacted specimen is shown in Figure 4b. The reacted microfilaments were comprised of fine particles (tens of nm in diameter). TEM/EDX analyses (Figure 4c) revealed that these fine particles contained magnesium and oxygen, with very little silicon detected throughout the reacted filament cross-sections (note: the small carbon and copper peaks in Figure 4c were generated by the substrate used to support the specimen during TEM analyses). A small amount of solidified Mg-Si liquid can be seen on the outside surfaces of a few converted MgO microfilaments in Figure 4a. Most of the Mg-Si liquid product migrated away from the MgO and onto the underlying steel substrate. An ED pattern obtained from the Mg-O nanoparticles is shown in Figure 4d. This and other ED patterns obtained from this specimen were consistent with the structure of periclase (MgO). The lattice parameter obtained from the ED patterns was 4.28 Å, which was comparable to the value of 4.22 Å reported for periclase.[6] These SEM, TEM, EDX, and ED analyses confirmed that: i) the biosculpted silica was fully converted into nanocrystalline magnesia within 4 hours at 900°C, and ii) the starting, biosculpted shape and fine features were preserved upon such conversion.

In order to capture the micro/nanostructural evolution during the course of the net reaction (1), subsequent experiments were conducted at lower reaction temperatures and for shorter reaction times. A secondary electron image of *Aulacoseira* frustules after exposure to Mg(g) for only 0.5 h at 750°C are shown in Figure 5a. Although these reacted frustules have a relatively granular appearance, the cylindrical frustule shape and fingerlike extensions were again preserved after such reaction. A TEM image of a cross-section of such a reacted frustule

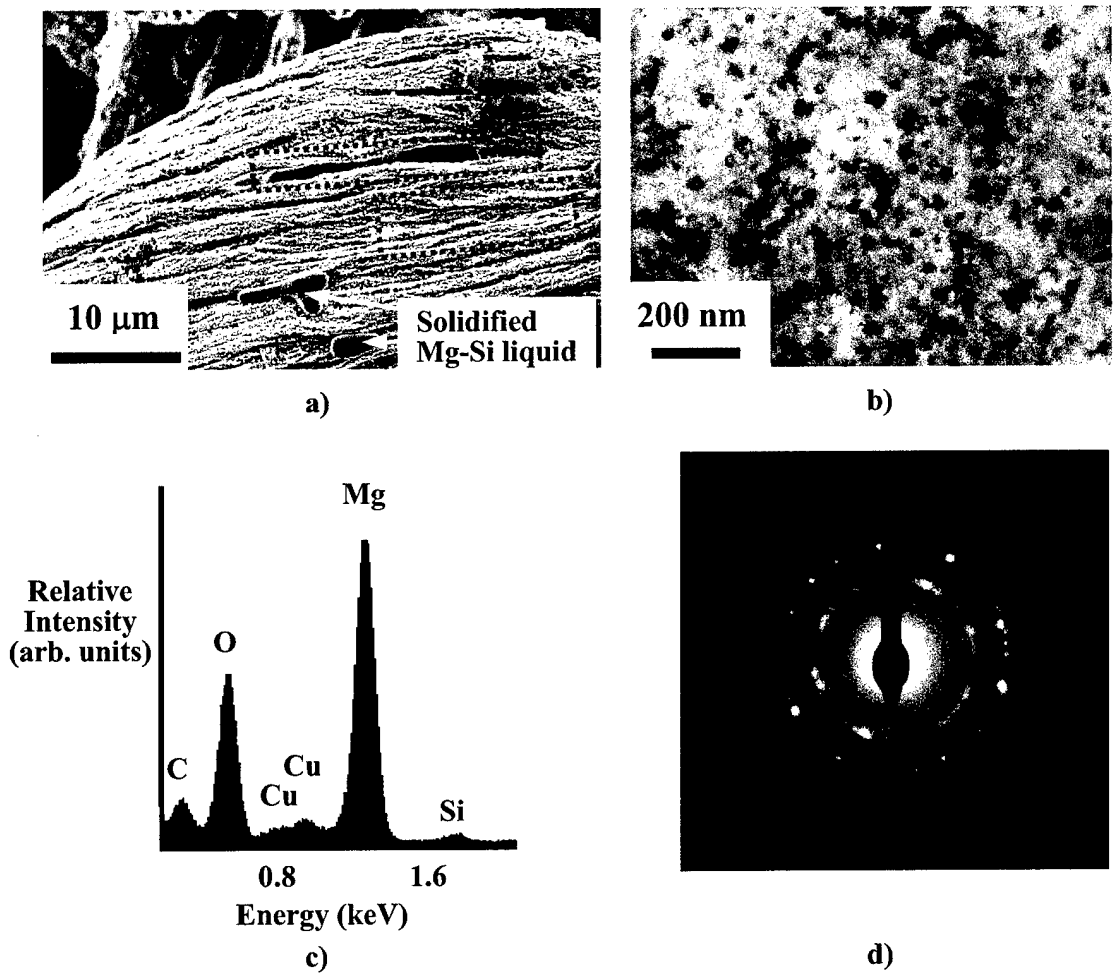


Figure 4. a) Secondary electron image of the same biosculpted microfilamentary silica shown in Fig. 2a) after reaction with Mg(g) at 900°C for 4 hours (fine features common to the starting and converted structures can be seen in the red boxes). b) Brightfield TEM image of a cross-section of a filament from the converted specimen in a). c) Energy-dispersive x-ray (EDX) spectrum and d) electron diffraction (ED) pattern obtained from TEM analyses of a cross-section of a biosculpted microfilament after reaction with Mg(g) at 900°C for 4 hours. The C and Cu peaks in the EDX pattern were generated by the carbon-coated copper grids used to support the specimens during TEM analyses.

(located near a pore channel) is shown in Figure 5b. Nanocrystallites with a relatively fine average size (i.e., finer than the MgO crystallites generated after 4 hours at 900°C, as shown in Figure 3f) can be seen on both sides of a pore channel. Elemental Mg and Si x-ray maps of a cross-section of a frustule exposed to the 750°C/0.5 hour treatment are shown in Figures 5c and 5d, respectively. The Mg map reveals the presence of magnesium throughout the thickness of the reacted frustule wall, which was consistent with the formation of MgO. EDX analyses (Figure 5e) obtained midway through the thickness of the frustule wall revealed strong peaks for magnesium and oxygen, with very little silicon detected. The Si map in Figure 5d reveals a Si-rich phase on the inner and outer surfaces of the reacted diatom wall, as well as within pore channels running through the thickness of the wall. These latter observations were consistent

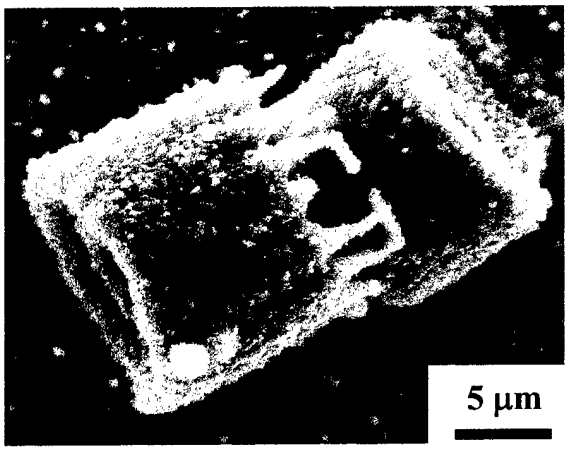


a)

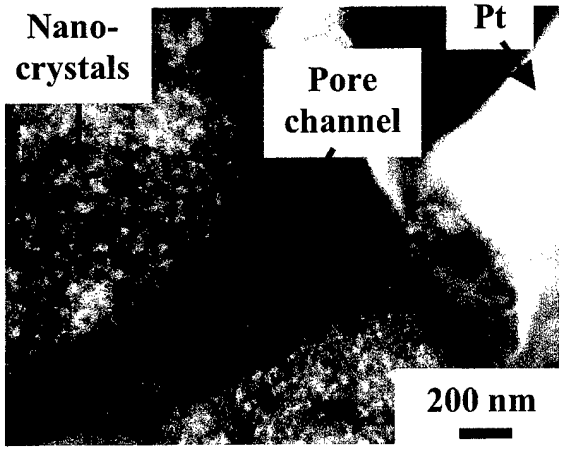


b)

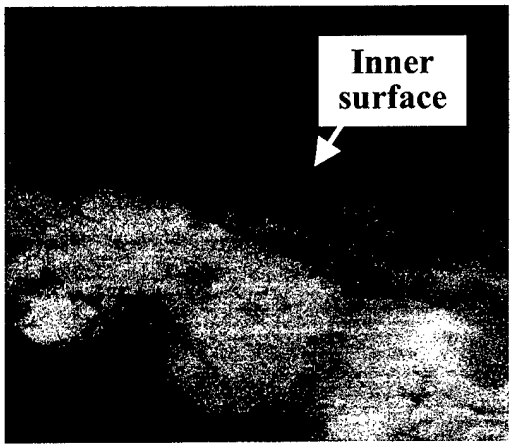


c)

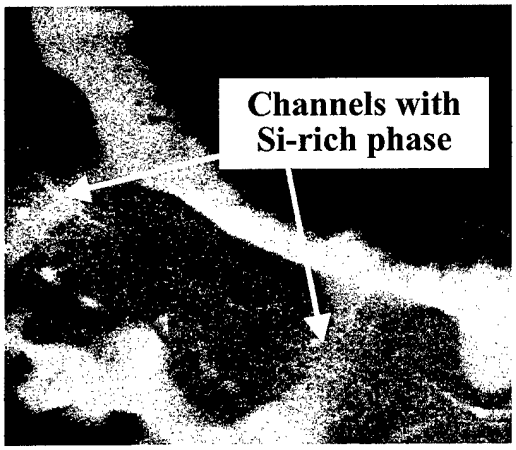


d)

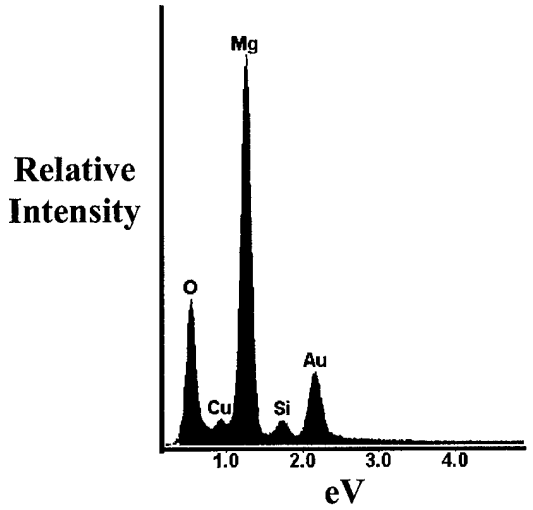


e)

Figure 5. a) Secondary electron (SE) image of an *Aulacoseira* frustule after exposure to Mg(g) at 750°C for 0.5 hours. b) TEM image and lower-magnification x-ray maps of c) Mg and d) Si obtained from a cross-section of an *Aulacoseira* frustule after the 750°C/0.5 hours treatment. e) Energy-dispersive x-ray (EDX) analysis midway through the wall of the 750°C/0.5 hours reacted frustule. (Note: Cu peaks in the EDX patterns were associated with the TEM grid; the Au peak resulted from a coating placed on the specimen to avoid charging.)

with Mg-Si liquid that was in the process of dewetting and leaving through the pores channels in the reacted frustule (note: a Mg-rich eutectic exists in the Mg-Si system at only 638°C.[5]). These maps (along with TEM/EDX analyses) indicated that the reaction was completed within just 0.5 hours at only 750°C.

Experiments were then conducted for a similar time at 700°C and 650°C. A secondary electron image of a frustule after exposure to the Mg(g) at 700°C for 0.5 hours is shown in Figure 6a. The overall shape and fine features (rows of pores, channels between interlocking

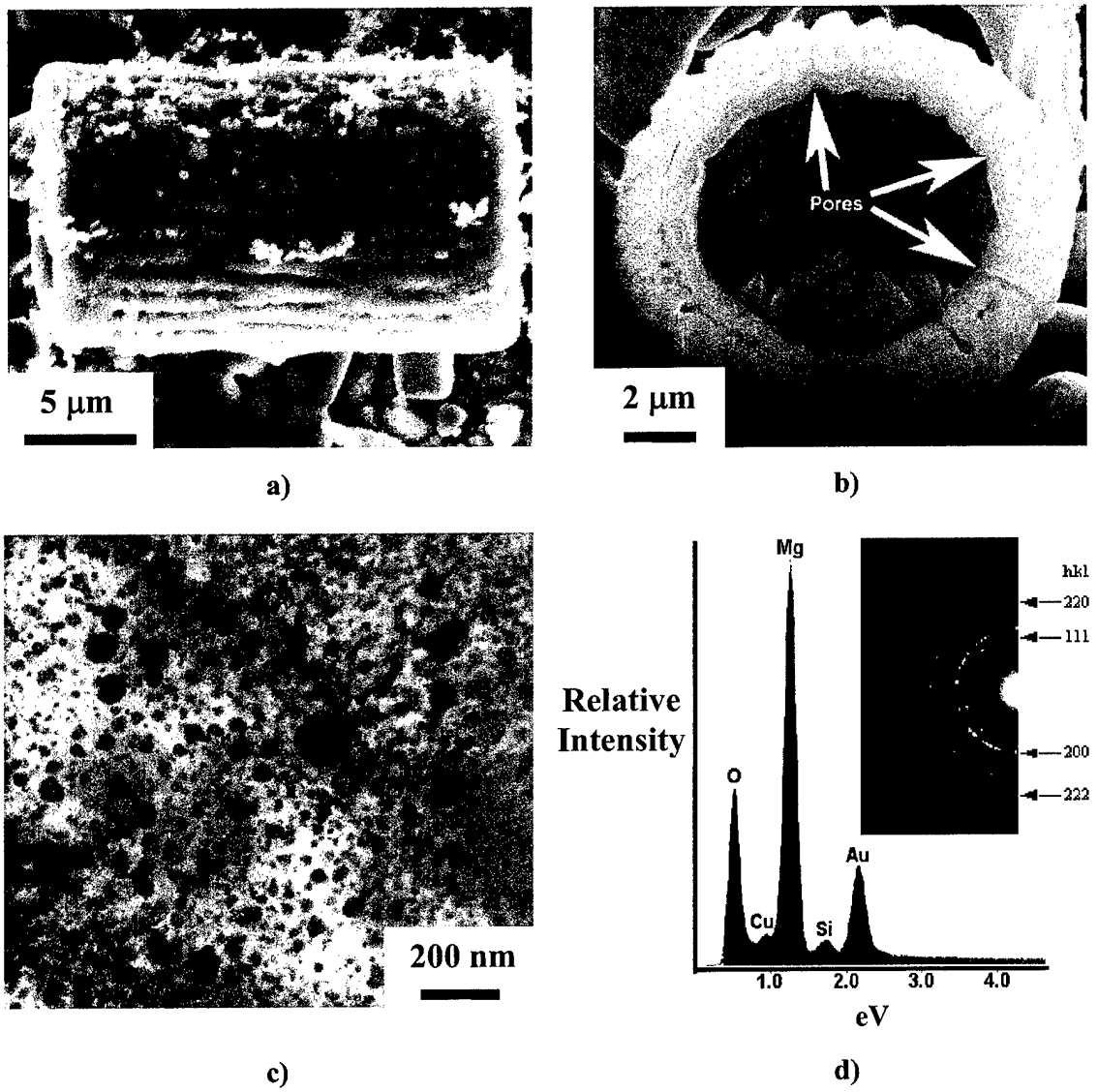


Figure 6. a) Secondary electron (SE) image of an *Aulacoseira* frustule after exposure to Mg(g) at 700°C for 0.5 hours. b) SE image of an ion-milled cross-section of the specimen in a). c) Dark field TEM image and d) EDX analysis, and electron diffraction (ED) analysis obtained from a cross-section of an *Aulacoseira* frustule after exposure to Mg(g) at 700°C for 0.5 hours. (Note: the Cu peak in the EDX pattern was associated with the TEM grid; the Au peak resulted from the coating placed on the specimen to avoid charging.)

fingerlike extensions) of the starting frustule were well preserved after this 700°C treatment. An ion milled, electron transparent cross-section of this specimen is shown in Figure 6b. A TEM image (Figure 6c) of this cross-section revealed fine crystals (most on the order of 50 nm in size or smaller). EDX analyses throughout the reacted frustule wall yielded predominant peaks for Mg and O, with little residual Si detected (Figure 6d). The near complete loss of silicon from the reacted frustules was also consistent with the presence of solidified pools of Mg-Si liquid detected below the frustules (see Figure 6a). Electron diffraction analyses at various locations through the wall of this reacted frustule yielded patterns consistent with the stable periclase polymorph of MgO (see the inset in Figure 6d). Hence, complete conversion of the silica-based *Aulacoseira* frustules into magnesia was also achieved within 0.5 hours at 700°C.

A different result was obtained with a 0.5 hour exposure of the *Aulacoseira* frustules to Mg(g) at 650°C. TEM analyses (Figure 7a) revealed a reacted microstructure with even finer crystallites than after the 700°C/0.5 hour treatment. EDX analyses of such reacted cross-sections revealed the presence of appreciable silicon, along with magnesium (Figure 7b). The retention of a significant silicon content within the wall of the frustule indicated that the reaction was not completed at this temperature within 0.5 hours. ED analyses (Figure 7c) of this specimen revealed a distinctly different pattern than for the specimen reacted at 700°C. The diffraction rings detected in this analysis were consistent with the compound forsterite, $Mg_2SiO_4$. The detection of $Mg_2SiO_4$ in the partially-reacted 650°C specimen, and the absence of this phase in the fully-reacted 700°C specimen, indicated that forsterite was an intermediate phase that formed in advance of the stable periclase (MgO) phase. Hence, this work indicates that the conversion of $SiO_2$ into MgO via the net reaction (1) proceeds through the following intermediate reactions:

$$Mg(g) + SiO_2(s) \Rightarrow \tfrac{1}{2}\, Mg_2SiO_4(s) + \tfrac{1}{2}\, \{Si\} \qquad (1a)$$

$$Mg(g) + \tfrac{1}{2}\, Mg_2SiO_4(s) \Rightarrow 2MgO(s) + \tfrac{1}{2}\, \{Si\} \qquad (1b)$$

Net reaction:
$$2Mg(g) + SiO_2(s) \Rightarrow 2MgO(s) + \{Si\} \qquad (1)$$

## III. Reactive Conversion of Bioclastic Silica into Calcium Oxide

$SiO_2$-based *Aulacoseira* diatom frustules were sealed with Ca(s) inside iron ampoules using a similar procedure as discussed in the previous section. The specimen-bearing ampoules were then heated to 1000-1200°C for times of 0.5-8 hours in a flowing argon atmosphere. Under these conditions, the calcium melted, vaporized, and then underwent the following net oxidation/reduction reaction:

$$2Ca(g) + SiO_2(s) \Rightarrow 2CaO(s) + \{Si\} \qquad (2)$$

Because the equilibrium vapor pressure of Ca(g) over Ca(l) is lower than for Mg(g) over Mg(l) at any given temperature, a higher temperature range of 1000-1200°C was selected for reaction (2) (the vapor pressure of Ca(g) over Ca(l) at 1200°C is 98 torr, which is similar to the 120 torr vapor pressure of Mg(g) over Mg(l) at 900°C[4]). Initial experiments were conducted at 1200°C for 8 hours. XRD analyses of these reacted frustules (Figure 8a) indicated that the silica had been converted into a mixture of CaO and $Ca_2Si$. While these reaction products were analogous to the MgO and $Mg_2Si$ products observed for the net reaction (1) at 900°C (see Figure 3e), SEM analyses (Figure 8b) indicated that the diatom frustule shape was not preserved after the prolonged 1200°C heat treatment. EDX analyses (Figure 8c) indicated that an appreciable amount of silicon was still retained within these

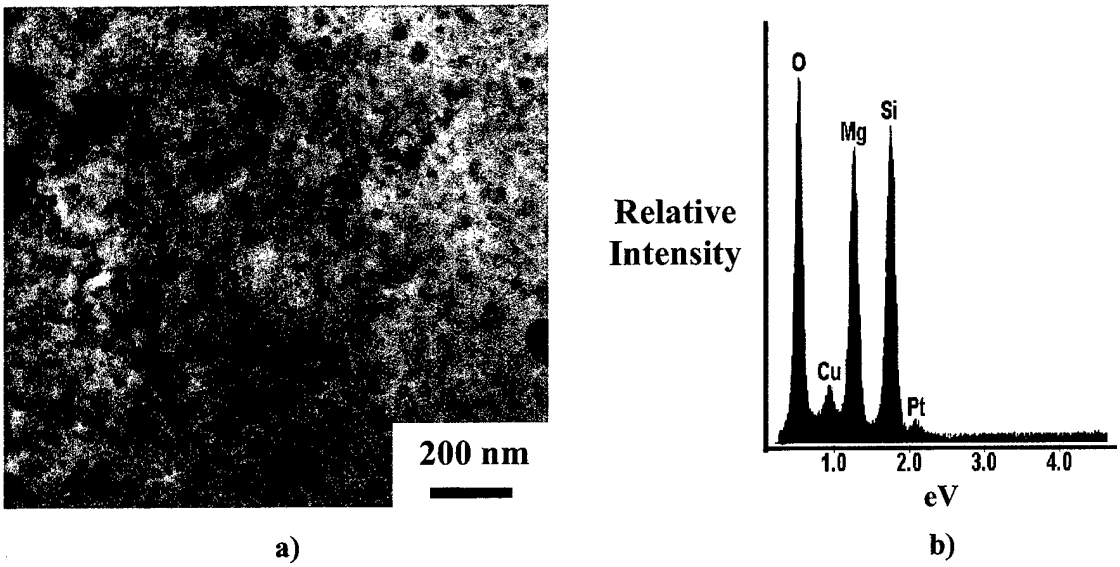


Figure 7. a) TEM image of a cross-section of an *Aulacoseira* frustule after exposure to Mg(g) at 650°C for 0.5 hours. b) EDX analysis and c) ED) analysis obtained from such a cross-section (note: Cu peaks in the EDX patterns were associated with the TEM grid; the Pt peak resulted from a coating placed on the specimen to avoid charging.)

distorted structures. While the compound $Mg_2Si$ melts congruently at 1085°C, the compound $Ca_2Si$ melts congruently at 1314°C (Figure 8d).[7] Although the Ca-Si phase diagram indicates that a Ca-rich liquid should form upon continued exposure of the $Ca_2Si$ compound to excess Ca(g) (a Ca-rich, Ca-Si eutectic exists at 792°C in the Ca-Si system[7]), the dissolution of the relatively refractory $Ca_2Si$ compound in this liquid, and migration of the liquid out of the CaO frustule, was quite sluggish at 1200°C.

An alternate, two-step process was developed to avoid the formation of the relatively

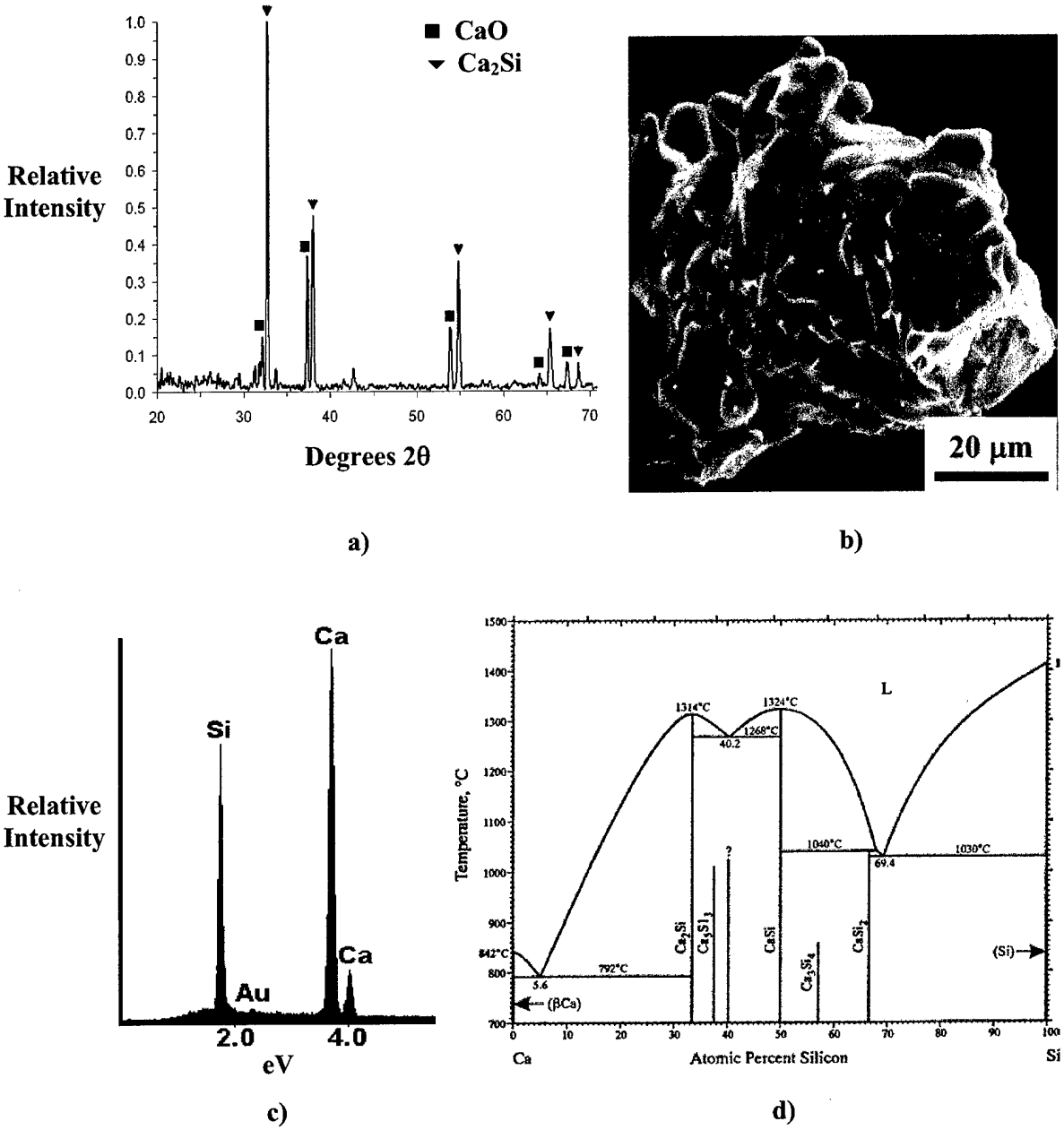


Figure 8. a) XRD analysis of *Aulacoseira* frustules after exposure to Ca(g) at 1200°C for 8 hours. b) Secondary electron (SE) image and c) energy-dispersive x-ray (EDX) analyses of an *Aulacoseira* frustule after exposure to Ca(g) at 1200°C for 8 hours. d) The Ca-Si binary phase diagram[7].

refractory $Ca_2Si$ compound so as to yield shape-preserved, pure CaO frustules. The silica preforms were first converted by reaction (2a) into MgO.

$$2Mg(g) + SiO_2(s) => 2MgO(s) + \{Si\} \quad (2a)$$

During this step, the silicon drained away quickly, as a low-melting Mg-Si liquid, from the MgO frustules. The MgO frustules were then exposed, in the second step, to Ca(g) to allow for the following displacement reaction:

$$Ca(g) + MgO(s) => CaO(s) + \{Mg\} \quad (2b)$$

where {Mg} refers to magnesium dissolved in a Mg-Ca liquid. Because all Ca-Mg compositions are completely molten above 842°C, the Mg-bearing product of this reaction could not be retained as a solid phase at reaction temperatures in excess of 842°C.[8] For this two-step process, the conditions for the first reaction (2a) were fixed at 900°C for 4 hours. These conditions were chosen based on prior work which revealed good preservation of the frustule shape and complete removal of the Si as an Mg-Si liquid from the MgO structures produced under these conditions. The second reaction (2b) was conducted over the temperature range of 1000-1200°C for times ranging from 0.25-8 hours.

EDX analysis of a MgO-converted frustule that had been exposed to Ca(g) at 1200°C for 0.25 hours is shown in Figure 9a. Little Si or Mg was detected on this converted frustule, which indicated that the reaction had been completed and that calcium silicide formation had been avoided. However, a secondary electron image of this CaO-based frustule (Figure 9b) indicated that this thermal treatment resulted in extensive coarsening of the frustule, so that the fine features of the starting silica-based frustule were not preserved. Experiments were then conducted using lower temperatures for the second step of the conversion process. Secondary electron images of the same MgO-converted frustule before and after exposure to Ca(g) at 1100°C for 0.25 hours are shown in Figures 9c and d, respectively. Comparison of these figures revealed that the general shape and fine features of the starting MgO frustule were preserved, although some coarsening had occurred. EDX analysis (Figure 9e) of the converted frustule in Figure 9d revealed a predominance of Ca, with very little Mg or Si detected, which indicated that the conversion to CaO had been largely completed within 0.25 hours at 1100°C. A further reduction in the CaO-conversion temperature to 1050°C for 0.25 hours resulted in limited conversion of the MgO into CaO, as revealed by the EDX analysis in Figure 9f.

A prolonged (8 hour) exposure to Ca(g) at 1000°C was then conducted with the intent of achieving complete conversion into CaO with reduced coarsening. Secondary electron images of the same frustules before and after conversion of the MgO into CaO are shown in Figures 10a and b, respectively. Although some coarsening was still observed, the overall shape and features of the MgO-converted frustule were preserved in the CaO structure. XRD analysis (Figure 10c) and EDX analysis (Fig. 10d) indicated that the conversion of MgO to CaO was largely completed within 8 h at 1000°C. While additional optimization may be conducted to further reduce coarsening, this work demonstrates that a two-step conversion process ($SiO_2$ -> MgO -> CaO) may be used to convert biosilica-based preforms into calcium oxide-based structures with a preservation of the starting preform shape and fine features.

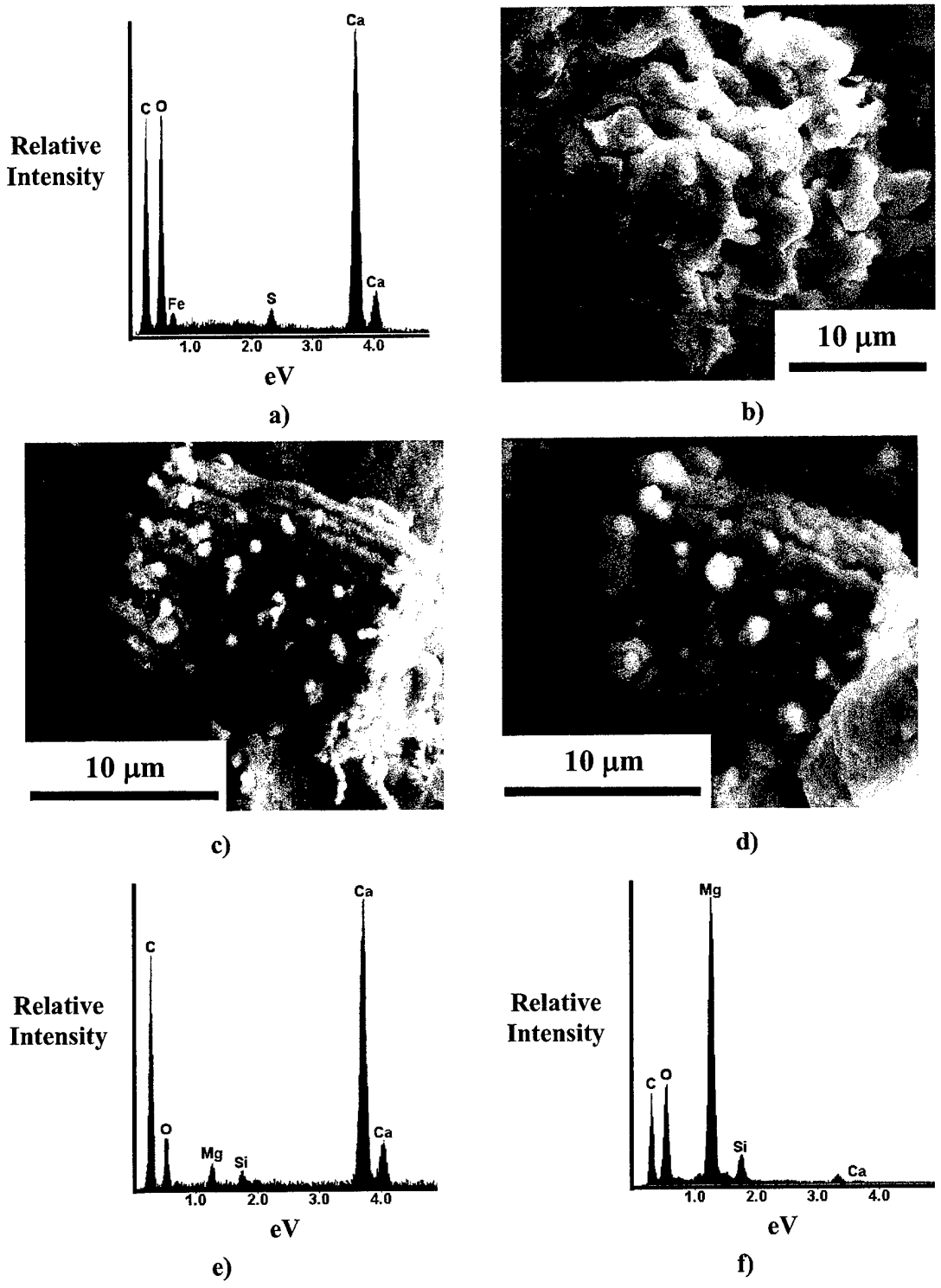


Figure 9. a) EDX analysis and b) SE image of an MgO-converted *Aulacoseira* frustule after exposure to Ca(g) at 1200°C for 0.25 h. c), d) SE images of the same MgO-converted *Aulacoseira* frustule before and after exposure to Ca(g) at 1100°C for 0.25 h. e), f) EDX analyses of MgO frustules after exposure to Ca(g) for 0.25 h at 1100°C and 1050°C, respectively.

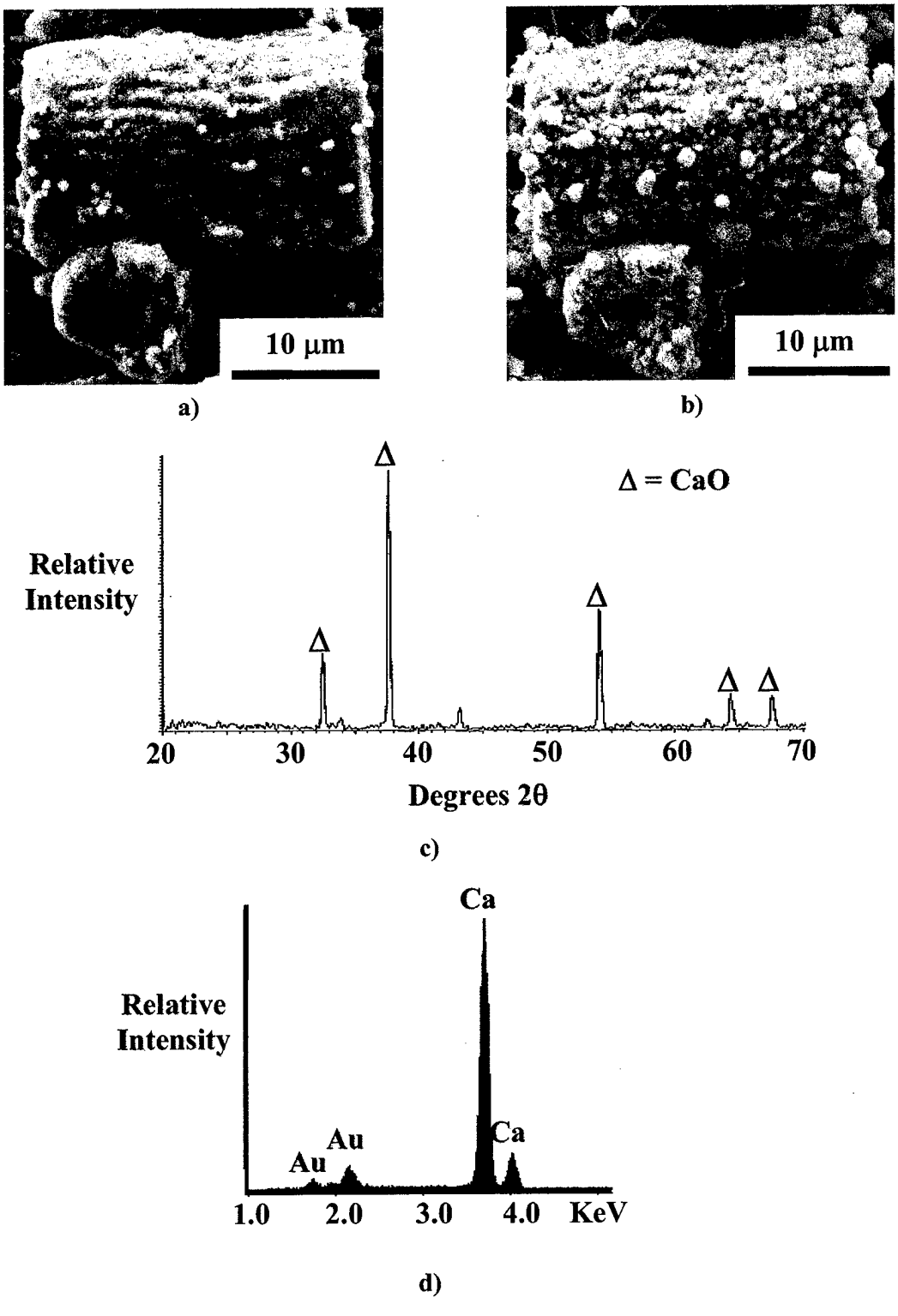


Figure 10. Secondary electron images of MgO-converted frustules a) before and b) after exposure to Ca(g) for 8 hours at 1000°C. c) XRD analysis and d) EDX analysis of the structures generated upon exposure to Ca(g) for 8 hours at 1000°C.

## IV. Reactive Conversion of Bioclastic Silica into Titanium Oxide

The following net metathetic reaction was examined for converting silica-based diatom frustules into titania:

$$TiF_4(g) + SiO_2(s) \rightarrow TiO_2(s) + SiF_4(g) \qquad (3)$$

Solid $TiF_4$ was utilized as a low-temperature source of $TiF_4$ vapor (note: the sublimation temperature of $TiF_4(s)$ is 285°C[4]). 100 milligrams of *Aulacoseira* diatom frustules were placed within a titanium tube (2.5 cm dia., 20 cm long) along with solid $TiF_4$. Both ends of the tube were then crimped and welded shut. The specimen-bearing tube was heated to the desired reaction temperature at 5°C/min and held for 2 h. At the end of this treatment, the tube was pushed out of the hot zone of the horizontal tube furnace. The tube was then cut open and the specimens were extracted. Some of these specimens were given a second heat treatment at 350°C for 2 h in pure, flowing oxygen.

Initial reaction experiments were conducted for 2 h at 500-700°C using $TiF_4$:$SiO_2$ molar ratios of $\geq$4.9:1 within the sealed titanium tubes (i.e., well in excess of the one-to-one ratio of $TiF_4$ to $SiO_2$ shown in reaction (3)). Figures 11a-c reveal secondary electron images of *Aulacoseira* frustules after exposure to $TiOF_2(g)$ at 600°C for 2 hours. The frustules were

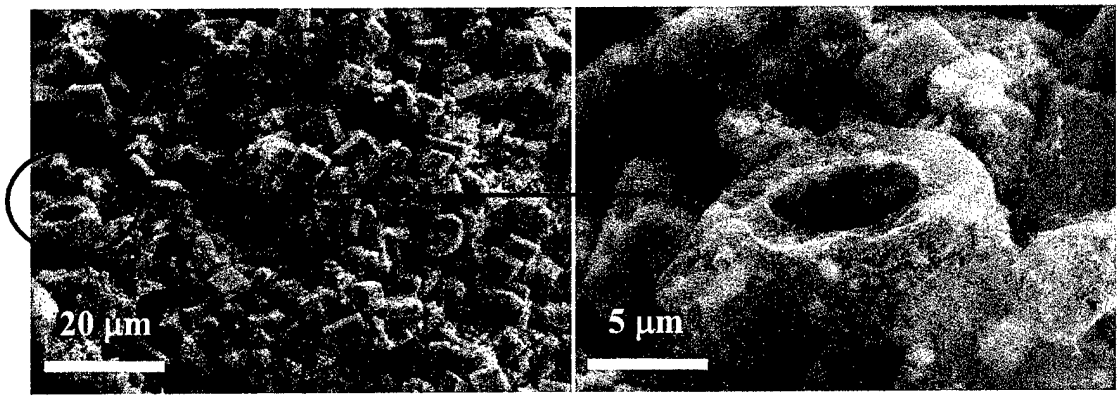


a) b)

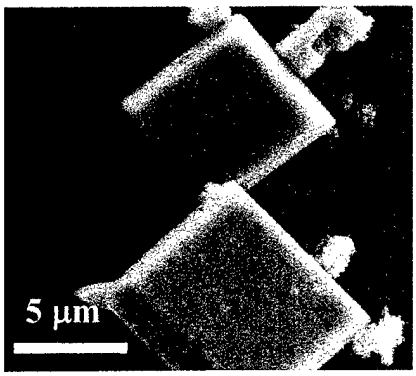


c)

Figure 11. a), b), c) Secondary electron (SE) images of *Aulacoseira* diatom frustules after exposure to $TiOF_2(g)$ for 2 h at 600°C.

gradually consumed under this condition (Figure 11b) and coarse, plate-shaped rutile ($TiO_2$) crystals formed nearby (Figure 11c). Similar results were obtained at reaction temperatures of 500°C and 700°C. Because the formation of titania occurred away from the frustule surface, the frustule shape was not preserved under these conditions.

A strikingly different result was obtained upon lowering the reaction temperature to 350°C and reducing the $TiF_4$:$SiO_2$ molar ratio to 2.4:1 within the titanium tubes. A secondary electron image of an *Aulacoseira* frustule exposed to $TiF_4$(g) under these conditions is shown in Figure 12b. The overall shape and fine features of the reacted frustule were quite similar to those of the starting frustules (such as shown in Figure 12a). Energy-dispersive x-ray (EDX) analyses revealed the presence of appreciable titanium, fluorine, and oxygen in such reacted frustules (Figure 13a). (Note: the peaks for Al, Au, and Pd in Figures 13a and 13c were generated by the

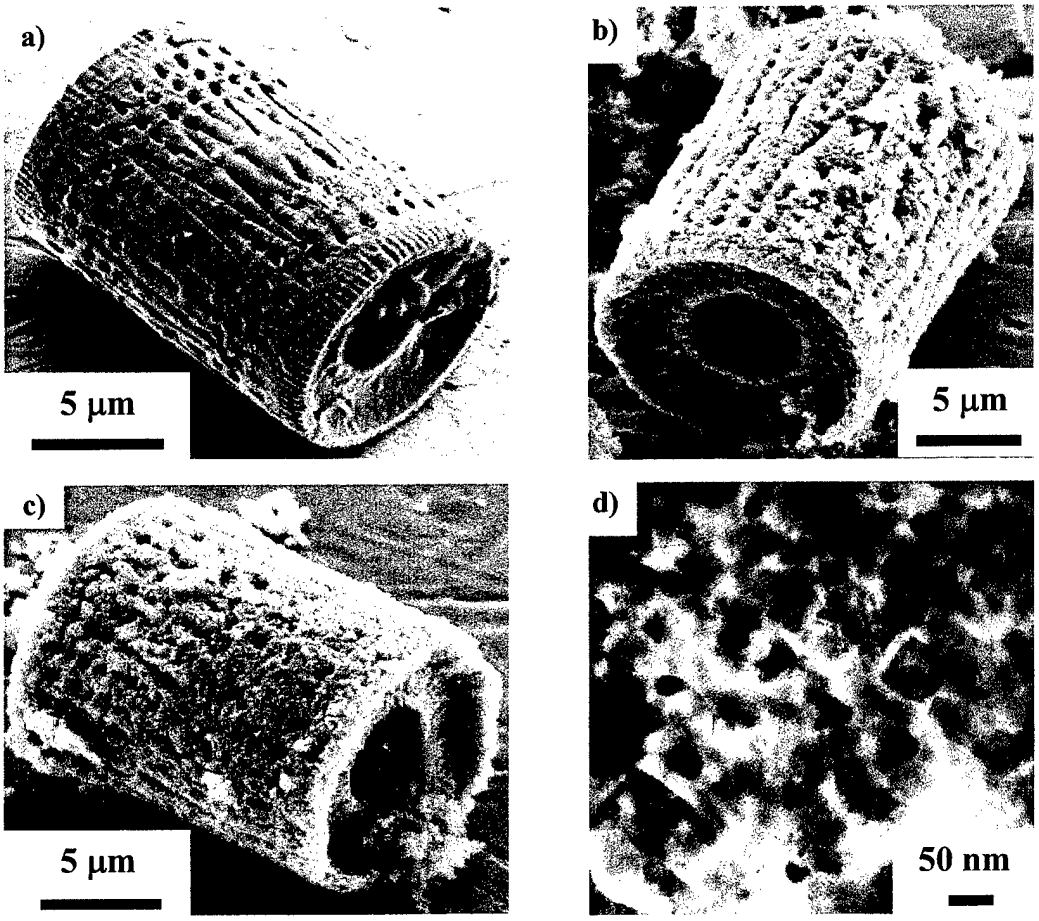


Figure 12. Secondary electron images of a) an *Aulacoseira* diatom frustule, b) an *Aulacoseira* frustule after exposure to $TiF_4$(g) for 2 h at 350°C, and c) an *Aulacoseira* frustule after exposure to $TiF_4$(g) for 2 h at 350°C and then to pure $O_2$(g) for 2 h at 350°C. d) A transmission electron image of a cross-section of a frustule after exposure to $TiF_4$(g) for 2 h at 350°C and then to pure $O_2$(g) for 2 h at 350°C.

aluminum substrate on which the specimens were placed and by the gold-palladium coating applied to the specimens to avoid charging.) The predominant EDX peak for silicon (1.74 keV) was not detected after this reaction treatment. X-ray diffraction (XRD) analyses of these reacted frustules (Figure 13b) indicated that the diatom silica had been converted into predominantly $TiOF_2$ along with a small amount of the anatase polymorph of $TiO_2$. Possible metathetic $TiF_4(g)/SiO_2(s)$ reactions that could have yielded $TiOF_2$ include:

$$TiF_4(g) + 1/2\ SiO_2(s) \rightarrow TiOF_2(s) + 1/2\ SiF_4(g) \quad (4)$$

$$TiF_4(g) + 2/3\ SiO_2(s) \rightarrow TiOF_2(s) + 1/3\ Si_2OF_6(g) \quad (5)$$

$$TiF_4(g) + SiO_2(s) \rightarrow TiOF_2(s) + SiOF_2(g) \quad (6)$$

Although it is not yet clear which of these was the predominant reaction, the standard Gibbs free energy changes for reactions (4) and (5) are considerably more negative than for reaction (6).[4,9]

Further heat treatment was conducted in flowing oxygen in order to convert the titanium oxyfluoride frustules into titanium oxide by the following net reaction.

$$TiOF_2(s) + \tfrac{1}{2}\ O_2(g) \rightarrow TiO_2(s) + F_2(g) \quad (7)$$

After exposure of the oxyfluoride-rich frustules to oxygen at 350°C for 2 h, the *Aulacoseira* frustule shape was still well preserved (Figure 12c). EDX analysis (Fig. 13c) indicated that the fluorine had been largely removed from the frustules by this treatment. Indeed, the predominant phase detected within these frustules by XRD analysis was the anatase polymorph of $TiO_2$ (Figure 13d). Anatase is a metastable form of $TiO_2$ that has often been found to form in advance of the stable polymorph, rutile. Such anatase formation is attractive in that anatase is a desired titania polymorph for certain gas sensor applications. A transmission electron microscope (TEM) image of an electron transparent cross-section of such an oxygen-treated specimen is shown in Figure 12d. This specimen consisted of a porous network of fine oxide crystals (<100 nm in size). Electron diffraction (ED) analyses (Figure 13e) of these nanocrystals were consistent with the tetragonal crystal structure of anatase.[6] Silicon was not detected throughout the frustule cross-section, which indicated that the conversion to anatase had been completed within 2 hours at 350°C.

This work demonstrates for the first time that a metathetic halide gas/solid reaction may be used to convert a biologically self-assembled 3-D structure into a new nanocrystalline material without a loss of the bioclastic shape or fine features. Although this work has focused on the conversion of diatom silica into the technologically-important oxide, titania, this approach may be conducted with other bioclastic or biomimetic preforms and with other thermodynamically-favored metathetic reactions to generate 3-D assemblies with a wide variety of shapes and functional chemistries. Such shape-preserving metathetic reactions may also be conducted with synthetic (non-natural) micro/nano-assemblies. For example, the titania-conversion process of this paper could be applied to silica-based colloidal crystals, membranes, or structures obtained by silicon micromachining.

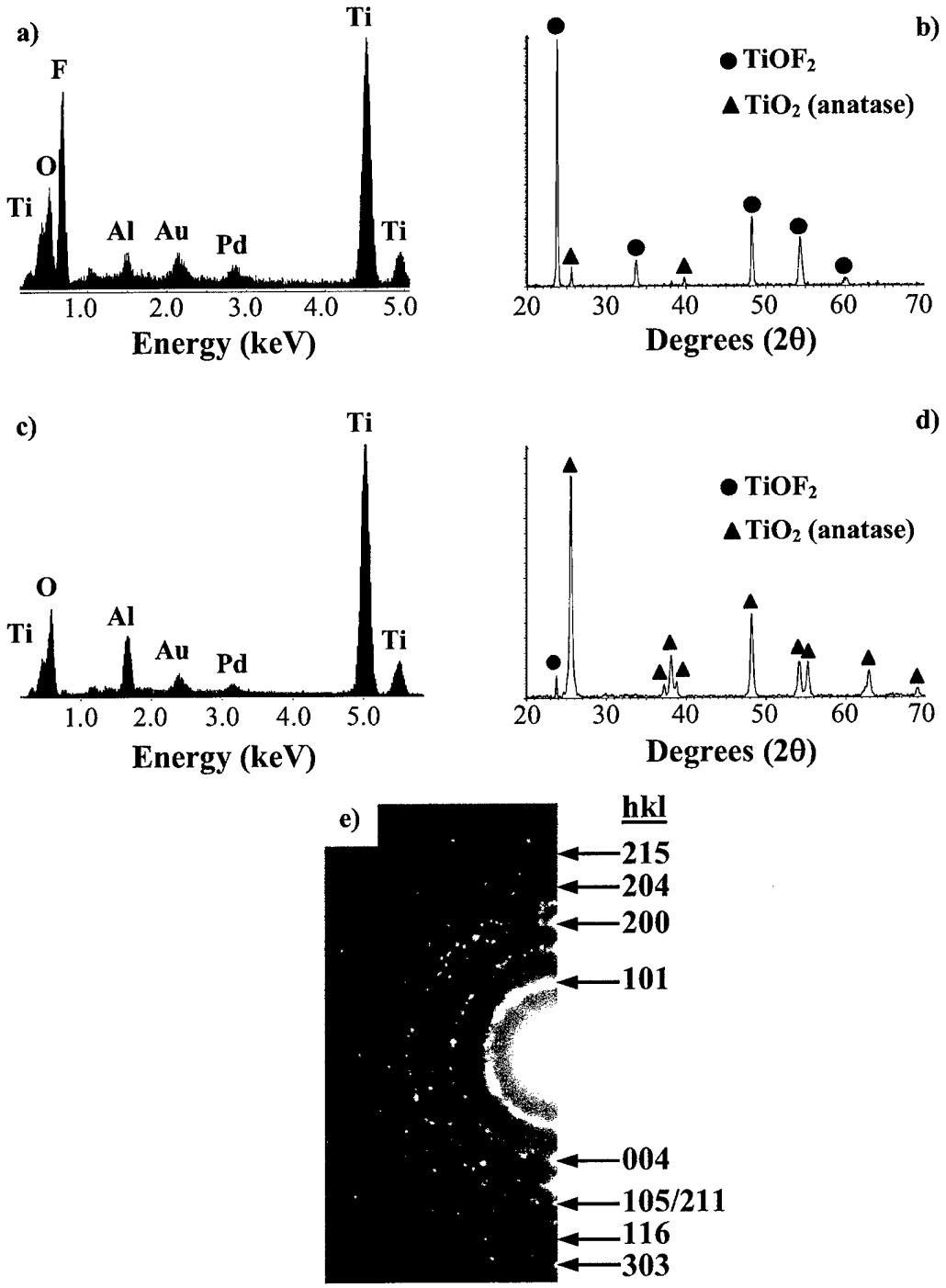


Figure 13. a) EDX analysis and b) XRD analysis of *Aulacoseira* frustules after exposure to $TiF_4$(g) for 2 h at 350°C. c) EDX analysis and d) XRD analysis of *Aulacoseira* frustules after exposure to $TiF_4$(g) for 2 h at 350°C and then to pure $O_2$(g) for 2 h at 350°C. e) TEM/ED pattern obtained from a cross-section of an *Aulacoseira* frustule after exposure to $TiF_4$(g) for 2 h at 350°C and then to pure $O_2$(g) for 2 h at 350°C (hkl values associated with diffraction from anatase are also shown[6]).

## V. Identification of Germania-forming Peptides

Through a strong collaboration with the Biotechnology Group (Rajesh Naik, Morley Stone, et al.) at the Air Force Research Laboratory at Wright-Patterson Air Force Base, progress has also been made in identifying peptides that promote the precipitation of germania. Such peptides are of interest for future *in vitro* biosculpting of germania-based assemblies with tailored shapes for potential optical devices for DoD applications. Furthermore, because germania possesses a Gibbs free energy of formation that is considerably smaller in magnitude than silica, a wider range of displacement reactions may be used to convert germania into other oxides than is possible with silica.

A commercially-available combinatorial peptide display library was used to identify peptides that exhibit strong binding to germania.[10-12] After several rounds of selective panning, 22 peptide-displaying phage clones with an enhanced affinity for germania were isolated. These peptides are listed in Table I below.

Table I: Sequences obtained of germanium binding peptides with amino acids having functional side groups in bold.

| Clone Number | Insert Sequence | pI* | Clone Number | Insert Sequence | pI* |
|---|---|---|---|---|---|
| 32 | **E**P**W**L**D**S**R**Y**S**PL**S** | 4.37 | 37 | **T**MGF**T**AP**R**FP**H**Y | 8.44 |
| 7 | G**H**GLLQ**Y**T**D**VMF | 5.08 | 8 | **S**LKMP**H**W**P**H**L**LP | 8.51 |
| r2 | **T**S**L**Y**T**D**R**P**ST**PL | 5.50 | r6 | **K**AWIV**Q**PPF**H**Y**S** | 8.60 |
| 36 | LPIP**SS**LGGPFP | 5.52 | 3 | **Q**LPK**H**N**Y**W**P**GAF | 8.60 |
| 4 | **SYE**MPF**STR**P**W**F | 5.72 | 6 | **YTTSNTLQ**VIA**R** | 8.75 |
| 2 | LPG**W**PLA**ER**VG**Q** | 6.00 | r4 | **NTPGIRPQATYS** | 8.75 |
| 34 | TG**H**Q**S**PGA**Y**AA**H** | 6.61 | 35 | AL**H**PL**T**N**R**H**Y**AT | 8.80 |
| 31 | NFME**S**LP**R**LGM**H** | 6.75 | r3 | **SNTSIIRN**AFPQ | 9.47 |
| r5 | **HSTW**KLL**R**LDME | 6.77 | 39 | GV**SQNTNSLHLR** | 9.76 |
| r8 | **H**ATGT**H**GL**S**L**S**H | 7.03 | r1 | GMV**STSR**M**H**AG**W** | 9.76 |
| r10 | **S**FL**YSYT**GP**R**PL | 8.31 | 1 | **S**V**S**VGM**K**P**S**P**RH** | 11.00 |

Preliminary experiments using a PCR method previously described[12] failed to yield any phage clones that remain attached to the germania particles after acid elution. This indicated that the acid elution was effective in releasing all of the germania-binding peptide displaying phages. The amino acid sequences of the displayed peptides were determined using DNA sequencing. The 3 most dominant peptides identified from the clones, labeled Ge2, Ge8, and Ge34 in Table II below, were chosen for further evaluation.

In order to assess the ability of these germania-binding peptides to promote germania precipitation, the peptides were introduced (1 $mg^{-ml}$) into a germanium alkoxide-bearing solution (0.135 M tetramethoxygermanium dissolved in methanol) at room temperature. Precipitation occurred rapidly upon introduction of either the Ge8 or Ge34 peptide into the alkoxide solution. In contrast, germania precipitation induced by the Ge2 peptide was difficult to detect by visual observation. Control experiments conducted with non-germania-binding peptides AG5[10] and AG-P28[12], or in the absence of the germania-binding peptides, failed to yield germania precipitates from the alkoxide solution. The extent of germania precipitation (i.e., the germania precipitating activity) was quantified by adapting the β-silicomolybdate colorimetric assay.[13] As shown in Figure 14, the Ge8 and Ge34 peptides exhibited relatively high germania-precipitating

**Table II.** Amino acid sequences and calculated isoelectric points of peptides used in this study.

| Peptide | Amino Acid Sequence | pI* |
|---|---|---|
| Ge2 | TSLYTDRPSTPL | 5.50 |
| Ge8 | SLKMPHWPHLLP | 8.51 |
| Ge34 | TGHQSPGAYAAH | 6.61 |
| AG5 | SLATQPPRTPPV | 9.47 |
| AG-P28 | SPLLYATTSNQS | 5.24 |

*pI calculated using pI/mass program at www.expasy.ch,

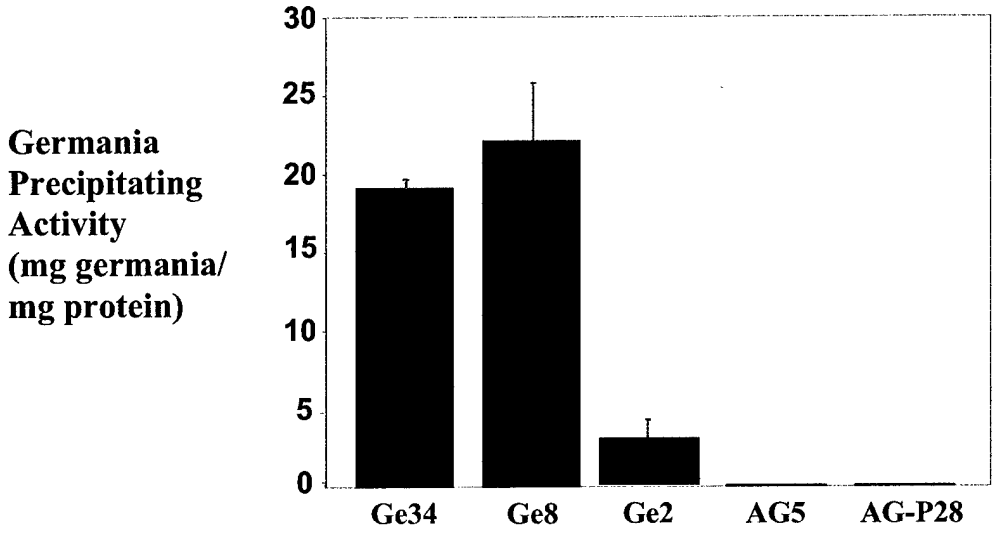


Figure 14. Germania precipitating activity of germania-binding and control peptides (milligrams of germania formed per milligram of peptide).

activities, whereas the Ge2 peptide exhibited much lower activity. The control peptides, AG5 and AG-P28, showed no germania precipitating activity.

The amino acids within peptides can provide molecular recognition motifs for strong binding to specific inorganic surfaces. The molecular characteristics that result in strong binding of a particular peptide to a specific inorganic surface may also enable that peptide to enhance the precipitation of the inorganic solid from a solution. The germania-binding peptides that were particularly effective in promoting germania precipitation from an alkoxide solution, Ge8 and Ge34, possessed hydroxyl- and imidazole-containing amino acid residues. The Ge8 peptide possessed a more basic isolectric point (pI), and a higher germania precipitating activity, than the Ge34 peptide. The germania-binding peptide with a low germania precipitating activity, Ge2, lacked histidine residues and possessed a more acidic pI. The failure of the control peptides AG5 and AG-P28 to produce germania indicated that precipitation in the presence of the germania-binding peptides was not a simple pH mediated hydrolysis but was instead specific to those sequences isolated by the panning process. It is worth noting that similar molecular

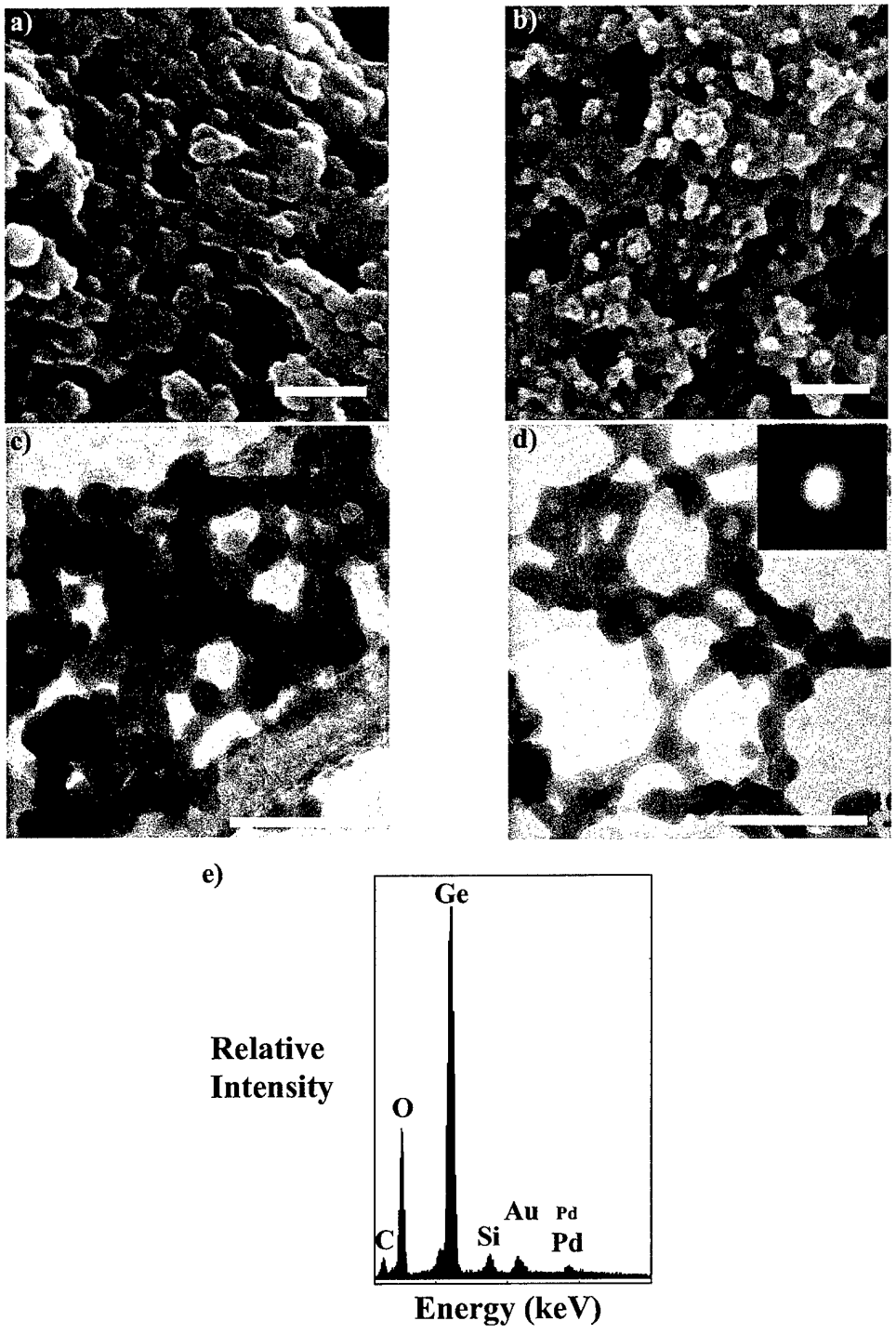


Figure 15. Germania nanoparticle networks precipitated from an alkoxide solution in the presence of germania-binding peptides. a), b) SEM images of germania formed in the presence of Ge8 and Ge34 peptides, respectively; c), d) TEM images of germania formed in the presence of Ge8 and Ge34 peptides, respectively; ED pattern of Ge34 precipitate (inset); e) EDX analysis of precipitate obtained using Ge34 peptide. Scale bar, 250 nm.

characteristics (hydroxyl- and imidazole-containing amino acid residues, basic pI) have been found in peptides that exhibited a high silica precipitating activity[8], although these silica-precipitating peptides were not among the 22 germania-binding peptides isolated in the present work.

The germania precipitates generated in the presence of either the Ge8 peptide or the Ge34 peptide were characterized by scanning electron microscopy (SEM) and transmission electron microscopy (TEM). SEM micrographs (Figures 15a, b) revealed that the precipitation products consisted of porous, inter-connected networks of agglomerates of fine particles. Energy dispersive x-ray (EDX) analyses revealed that the precipitates were enriched in germanium and oxygen (Figure 15e; the minor Au and Pd peaks were a result of the coating applied to the particles to avoid surface charge buildup in the SEM, and the minor Si peak was generated by the silicon substrate on which the precipitates were placed). High resolution TEM images (Figures 15c and 15d) confirmed the open network structures and revealed that the fundamental germania particles possessed diameters on the order of 50-100 nm. TEM analyses also revealed that the particle agglomerates contained regions of low density (relatively bright regions in Figures 15c and d), which consisted of either entrapped pores or residual organic material. Electron diffraction (ED) analyses obtained at numerous locations within the Ge8- and Ge34-induced precipitation products indicated that the germania was amorphous. The morphologies of germania precipitates formed in the presence of the Ge8 and Ge34 peptides were similar.

The combinatorial peptide display technique (so-called biopanning) can be a rapid and effective means of identifying peptides that will bind selectively to, and promote the rapid precipitation of, technologically-important solids for a host of electronic, biomedical, optical, chemical, sensor, and catalytic applications. In this work, we have used a phage display peptide library to identify germania-binding peptides that promote the rapid, room-temperature precipitation of amorphous germania nanoparticle networks from an alkoxide solution. It is likely that the chemistry, and resulting optical properties, of the germania-bearing precipitates can be adjusted by doping of the alkoxide precursor solution and/or by using combinations of peptides that promote the co-precipitation of germania with other oxides (e.g., germania-silica compositions for optical waveguides). The ability of such peptides to promote the *rapid, room-temperature precipitation of tailored oxide compositions*, coupled with the relative ease of peptide patterning on various surfaces, enables exciting new opportunities for the integration of functional oxides with low-temperature or reactive materials (e.g., polymer-, bio-organic-, or silicon-based devices).

## VI. References


1. N. Kroger, R. Deutzmann, M. Sumper, Science, **286**, 1129 (1999)
2. R. R. Naik, P. W. Whitlock, F. Rodriguez, L. L. Brott, D. D. Glawe, S. J. Clarson, M. O. Stone, Chem. Commun. 238 (2003)
3. A. A. Nayeb-Hashemi, J. B. Clark, L. J. Swartzendruber, Bull. Alloy Phase Diagrams, **6** [3] 235 (1985).
4. I. Barin, Thermochemical Data of Pure Substances, VCH Verlagsgesellschaft, Weinheim, Germany (1995)
5. R. Geffken, E. Miller, Trans. AIME, **242**, 2323 (1968)
6. Powder Diffraction File, Card Nos. 21-1272, 77-0132, 78-0430, International Centre on Diffraction Data, Newtown Square, PA

7. Binary Alloy Phase Diagrams, 2nd edition, edited by T. B. Massalski, H. Okamoto, P. R. Subramanian, and L. Kacprzak, ASM International, Materials Park, OH, 951, 953-954 (1990).
8. H. Okamoto, J. Phase Equilibria, **19** [5] 490 (1998).
9. M. Shinmei, T. Imai, T. Yokokawa, C. R. Masson, J. Chem. Thermodynamics, **18**, 241 (1986).
10. R. R. Naik, L. L. Brott, S. J. Clarson, M. O. Stone, J. Nanosci. Nanotech., **2**, 95 (2002).
11. R. R. Naik, S. J Stringer, G. Agarwal, S. E. Jones, M. O. Stone, Nature Mater., **1**, 169 (2002).
12. R. R. Naik, S. E. Jones, C. J. Murray, J. C, McAuliffe, R. A. Vaia, M. O. Stone, Adv. Func. Mater., **14**, 25 (2004).
13. R. K. Iler, The Chemistry of Silica, Wiley, New York (1979).

**VII. Other interactions include the following technical presentations (* = invited talk):**

1. (*) K. H. Sandhage, M. B. Dickerson, P. M. Huseman, F. M. Zalar, M. R. Rondon, E. C. Sandhage, "A Novel Hybrid Route to Chemically-Tailored, Three-Dimensional Oxide Nanostructures: The BaSIC (Bioclastic and Shape-Preserving Inorganic Conversion) Process," 26th Annual International Conference on Advanced Ceramics and Composites, Cocoa Beach, FL, Jan. 15, 2002.
2. (*) K. H. Sandhage, "3D, Self-Assembled Nanoparticle Structures with Tailored Chemistries via the BaSIC Process," Ceramics Colloquium talk, Univ. Illinois, April 11, 2002.
3. K. H. Sandhage. M. B. Dickerson, P. Huseman, F. M. Zalar, "A Novel, Bioclastic Processing Route to Complex-Shaped, 3-D Self-Assembled Nanoparticle Structures with Tailored Chemistries," presented in the Symposium on the Synthesis and Processing of Nanomaterials II, 104th Annual American Ceramic Society Meeting, St. Louis, MO, April 30, 2002.
4. (*) K. H. Sandhage, "Mass Production of 3-D, Self-Assembled Nanoparticle Structures with Tailored Chemistries via the BaSIC Process," presented to the Research and Development Division at the General Electric Corp., Schenectady, NY, May 13, 2002.
5. (*) K. H. Sandhage, M. B. Dickerson, P. M. Huseman, F. M. Zalar, G. Agarwal, R. R. Naik, M. O. Stone, M. E. A. Schoenwaelder, "A Novel Bioclastic Route to Complex-Shaped, 3-D Nanoparticle Structures with Tailored Chemistries for Biomedical Applications," presented at the Symposium on Advanced Materials for Biomedical Applications at the Conference of Metallurgists, Montreal, Canada, Aug. 13, 2002.
6. (*) K. H. Sandhage, F. M. Zalar, M. B. Dickerson, C. S. Gaddis, R. Naik, M. O. Stone, M. E. A. Schoenwaelder, "Chemically-Tailored, 3-D Nanoparticle Structures via the BaSIC Process," 8th International Conference on Ceramic Process Science, Hamburg, Germany, Sept. 4, 2002.
7. (*) K. H. Sandhage, F. M. Zalar, M. B. Dickerson, C. S. Gaddis, G. Agarwal, R. R. Naik, M. O. Stone, "A Novel Bioclastic Route to Self-Assembled, 3-D Nanoparticle Structures with Tailored Chemistries: the BaSIC Process," colloquium talk presented to the Materials Science and Engineering, University of Pennsylvania, Sept. 19, 2002
8. "Self-Assembled, 3-D Nanoparticle Structures with Tailored Chemistries via the BaSIC Process," F. M. Zalar, M. B. Dickerson, K. H. Sandhage, presented at the 11th International Symposium on the Processing and Fabrication of Advanced Materials, ASM/TMS Conference, Columbus, OH, Oct. 9, 2002.

9. (*) "Synthesis of Complex-Shaped, 3-D, Self-Assembled Nanoparticle Structures with Tailored Chemistries by the BaSIC Process," F. M. Zalar, M. B. Dickerson, R. R. Unocic, K. H. Sandhage, presented at the 2002 MRS Fall Meeting, Boston, MA, Dec. 5, 2002.
10. (*) "Chemically-Tailored, 3-D Nanoparticle Structures by the BaSIC Process," F. M. Zalar, R. R. Unocic, C. S. Gaddis, J. Zhao, K. H. Sandhage," presented at the 27th Annual American Ceramic Society Conference on Composites, Advanced Ceramics, Materials, and Structures, Cocoa Beach, FL, Jan. 30, 2003.
11. (*) "A Novel Bioclastic route to Self-Assembled, 3-D Nanoparticle Structures with Tailored Chemistries: the BaSIC Process," K. H. Sandhage, F. M. Zalar, R. R. Unocic, M. B. Dickerson, C. S. Gaddis, R. R. Naik, M. O. Stone, colloquium talk presented to the School of Materials Science Engineering, Georgia Institute of Technology, Atlanta, GA, March 10, 2003.
12. (*) "The BaSIC Route to 3-D Nanoparticle Structures with Tailored Chemistries," K. H. Sandhage, F. M. Zalar, R. R. Unocic, M. B. Dickerson, C. S. Gaddis, R. R. Naik, M. O. Stone, colloquium talk presented to the Dept. of Materials Science Engineering, Cornell University, Ithaca, NY, March 13, 2003.
13. "Low-Temperature, Shape-Preserving Chemical Conversion of Self-Assembled, 3-D Nanoparticle Structures: the BaSIC Process," K. H. Sandhage, M. B. Dickerson, P. M. Huseman, F. M. Zalar, presented at the 105$^{th}$ Annual Meeting of the American Ceramic Society, Nashville, TN, April 28, 2003.
14. "A Novel Bioclastic Route to Non-Oxide Ceramic Powder of Controlled Size and Shape," C. S. Gaddis, J. Zhao, K. H. Sandhage, presented at the 105$^{th}$ Annual Meeting of the American Ceramic Society, Nashville, TN, April 29, 2003.
15. (*) K. H. Sandhage, "Chemically-Tailored 3-D Nanoparticle Structures by the BaSIC (Bioclastic and Shape-preserving Inorganic Conversion) Process," presented at the Composites at Lake Louise Conference, Lake Louise, Canada, Oct. 21, 2003.
16. (*) K. H. Sandhage, M. B. Dickerson, P. M. Sarosi, G. Agarwal, R. R. Naik, M. O. Stone, "Chemical Transformation of Diatoms," presented in the Diatom Nanotechnology Workshop at the North American Diatom Society meeting, Florida Keys, October 22-26, 2003
17. C. S. Gaddis, J. Zhao, K. H. Sandhage, "A Transient Bioscaffolding Route to Chemically-Tailored, Nanoparticle-based Assemblies with Complex 3-D Shapes and Fine (Meso-to-Nanoscale) Features," presented at the Materials Research Society Fall Meeting, Boston, MA, Dec. 2, 2003.
18. R. R. Unocic, F. M. Zalar, K. H. Sandhage, "A Hybrid (Biogenic/Synthetic) Route to 3-D Nanoparticle Assemblies with Tailored Chemistries: The Bioclastic and Shape-preserving Inorganic Conversion (BaSIC) Process," presented at the Materials Research Society Fall Meeting, Boston, MA, Dec. 2, 2003.

**IX. Honors/Awards:** Fellow, The American Ceramic Society, 2002
Lumley Research Award, College of Engineering, Ohio State Univ., 2002

## Abstract:

This project has been aimed at: 1) identifying gas/solid reaction conditions for converting biologically-derived micro/nanotemplates into other oxides without a loss of the starting 3-D shape and fine features, and 2) evaluating the nanochemical/nanostructural evolution during such reactive conversion. The most significant accomplishments have been:

1) Development of an oxidation-reduction reaction process for converting biosilica-based micro/nanoassemblies into MgO nanoparticle structures with a preservation of the starting 3-D shape and fine features at temperatures as low as 700°C
2) Development of a two-step oxidation-reduction reaction process for converting biosilica-based micro/nanoassemblies into CaO nanoparticle structures with a preservation of the starting 3-D shape and fine features at temperatures as low as 1000°C
3) Development of a two-step metathetic reaction process for converting biosilica-based micro/nanoassemblies into $TiO_2$ nanoparticle structures with a preservation of the starting 3-D shape and fine features at temperatures as low as 350°C
4) Identification of novel reaction paths accessed during conversion of biosilica structures into magnesia (via formation of forsterite as an intermediate product) and titania (via formation of the intermediate compound, titanium oxyfluoride)
5) Identification of peptides that promote room-temperature formation of germania nanoparticle networks